Some Studies on Development of Ductile Conventional Cast Magnesium-Based Alloys

A

Project Report

submitted in partial fulfillment of the requirement for the award of the degree of

MASTER OF TECHNOLOGY

in

Production Engineering

by

GAURAV

Roll. No. 04/PRD/2K10

Under the guidance of

Mr. N. Yuvraj
Assistant Professor
DTU, New Delhi

Dr. K. L. Sahoo
Principal Scientist
CSIR-NML
Jamshedpur

DEPARTMENT OF MECHANICAL ENGINEERING
DELHI TECHNOLOGICAL UNIVERSITY
NEW DELHI-110042
JULY-2012

Department of Mechanical Engineering
Delhi Technological University
Delhi

CERTIFICATE

This is to certify that the thesis entitled ***"Some studies on development of ductile conventional cast magnesium-based alloys"*** submitted by **Gaurav**, during the session 2010-12 for the award of M.Tech. degree of Delhi Technological University, Delhi is absolutely based upon his work done at CSIR-National Metallurgical Laboratory, Jamshedpur under our supervision and guidance and that neither this thesis nor any part of it has been submitted for any degree /diploma or any other academic award.

The assistance and help received during the course of investigation have been fully acknowledged. He is a good student and we wish him good luck in future.

Mr. N. Yuvraj
Assistant Professor
Delhi Technological University
Delhi

Dr. K. L.Sahoo
Principal Scientist
CSIR-NML
Jamshedpur

ACKNOWLEDGEMENT

I like to express my deep sense of respect and gratitude to my mentors, Mr. N. Yuvraj, Department of Mechanical Engineering, Delhi Technological University, Delhi and Dr. K .L. Sahoo, Scientist, CSIR-National Metallurgical Laboratory, Jamshedpur, for their invaluable and fruitful constructive suggestions and guidance that have enabled me to overcome all the problems and difficulties while carrying out multi-functionaries of the present investigation. I feel fortunate for the support, involvement and well wishes of my mentors and this is virtually impossible to express them in words.

I express my sincere gratitude and indebtedness to Dr. Durbadal Mandal, Dr. Palash Poddar and Dr. S. Srikanth, Director, for extending their support, suggestion and giving me a chance to access all the facilities of the laboratory, required for my project/research work.

Although it is impossible to thank all the persons individually, I am especially thankful to Lakhi, Manoranjan ,Laxmi, S.S.Singh for their help and support.

I deeply acknowledge my indebtedness to my friends for their love, good wishes and continuous encouragement.

(**Gaurav**)
(04/PRD/2010)
M.Tech (Production Engineering)
Delhi Technological University

CONTENTS

LIST OF TABLES

LIST OF FIGURES

LIST OF FIGURES

LIST OF FIGURES

Abstract

Magnesium-based alloys have enormous potential for high performance structural applications due to their light weight combine with high specific strength, superior damping capacity, etc. Based on these superior properties and a combinative requirement for reducing environmental burdens by using light weighted stuructures, the research and development of magnesium alloys for practical industrial application have overwhelmingly increased worldwide during the past decade. AZ series cast Mg alloys have been extensively studied and used for some structural components of automobiles, aircraft, and computers. Alloying elements are partly present in solid solution, partly as intermetallic constituents. It is, however, interesting to see that there is a fairly good correlation between strength and total wt% of added elements. An effort has been made to develop a new Mg-alloy system that possesses exceptionally high ductility as well as good mechanical strength at room temperature in as-cast state. A novel Mg alloy system contains small amount of Al, Zn, Sn, Pb, Si and Misch metal (MM) has been developed for easy mechanical forming at room temperature .These are low-cost Mg alloys with improved tensile strength. The main alloy elements in the novel alloy system Sn and Pb are not expensive and the other alloy elements are either cheap and/or used in small amounts. Therefore, this new Mg alloy system is not expensive and may be produced at a large scale for a wide range of industrial applications. Microstructure evolution and resulting mechanical properties in Mg-Al-Zn-Pb-Sn based alloys have

been investigated. The microstructure of the studies alloys Mg-4Al-3Zn-3Sn-3Pb and Mg-4Al-3Zn-3Sn-3Pb-0.5misch metal (MM) are dendritic in nature while for Mg-3Zn-3Sn-3Pb-2Si the 'Chinese script' Mg_2Si intermetallic structure is obtained. Effect of MM on microstructure and mechanical properties as-cast Mg-4Al- 3Zn-3Sn-3Pb-0.5MM is maximum. The result shows that MM addition leads to obvious grain refinement. The UTS, YS, and percentage elongation of Mg-4Al-3Zn-3Sn-3Pb-0.5MM alloy are 170, 44 and 3.4%. The alloys investigated exhibit plastic deformation and work hardening during wear test. Specific wear rate (mm^3/N-m) or cumulative wear loss (mm^3) is found maximum for Mg-4Al-3Zn-3Sn- 3Pb-0.5MM. Addition of 4% Al, 3% Pb, 3%Sn, 3% Zn and 3% Si leads to Al-Sn, Al-Pb, Pb-Zn, phase in α-Mg matrix grains. The effects of alloying elements on Vickers hardness of alloys were examined. The vicker hardness value is found maximum for Mg-3Zn-3Sn-3Pb-2Si is 61 HV. The fracture surface of of Mg-Al-Zn-Sn-Pb alloys based system shows clearly ductile fracture evidence.

The growth of magnesium alloys is driven primarily by the automotive industry as structural material. Due to increasing environmental concerns and severe government regulations on CO_2 emissions, vehicle weight and fuel economy are becoming increasingly important in the automobile sectors. Therefore, the need of light weight metallic materials has led to significant consideration of materials researchers into Mg-alloys because of their low density and high specific strength. In the past few years, incremental use of Mg-alloys in automobile industry has been observed. Among Mg-alloys, Mg-Al alloys are the most promising for automotive industry because of their acceptable mechanical properties, good corrosion resistance and excellent cast-ability [1]. Magnesium alloys are finding increasing applications in industry mainly due to their high strength-to-weight ratio. Its specific tensile strength and rigidity are superior to Fe and Al. The greatest limitation for the usage of wrought Mg is its poor formability at room temperature due to its hexagonal closed packed (HCP) crystal structure; only three independent basal slip systems can be activated, all parallel to the basal plane (0001) [2]. However, the ductility of Mg can be greatly improved at high temperature due to the activation of non-basal slip systems. A fine grain structure and random texture will also improve the ductility of Mg due to the decrease of volume fraction of twinning and the increase number of basal slip systems that can be activated respectively. However, they have intrinsically poor plastic deformation ability at room temperature. Therefore, the vast majority of Mg alloys are used only in cast state, severely limiting the development of their applications.The mechanical properties of Mg can

be widely influenced by alloying. The strength of cast Mg-alloys is obtained by one or more of the well known hardening mechanisms: solid solution hardening, grain size or Hall Petch hardening, age hardening and dispersion hardening. Hence, the alloying elements are partly present in solid solution, partly as intermetallic constituents. It is, however, interesting to see that there is a fairly good correlation between strength and total wt% of added elements. The most common hardening elements are Al, Zn, Si, RE elements like Y and Ag exhibit a high solid solubility at high temperature and the solid solubility decreases with falling temperature.

Elevated temperature properties of Mg-based alloys can be improved by several ways. The most common way of improving the elevated temperature properties is the formation thermally stable precipitates or dispersoids along the grain boundaries to resists the deformation by grain boundary sliding [3]. As for example, Sn possesses several characteristics features such as low diffusivity in Mg ($10x10^{-14}$ m/s^2 at 400 ^oC), low solid solubility in Mg (0.035 at.% at room temperature) and high liquid solubility in molten Mg (100% at 800 ^oC). Moreover, the main phase in Mg-Sn alloys system, Mg_2Sn has a high melting temperature of about 770 ^oC. Thus, during solidification of the cast product thermally stable Mg_2Sn particles formed along the grain boundaries as well as grain interior. The use of RE elements to improve the elevated temperature of Mg-alloys is not economical due to its high cost and difficulties in achieving in homogeneous structure. The use of misch-metal (MM) (52%Ce-26%La-16%Nd-6%Pr) instead of individual RE elements is much economical since the cost of Mm is ~10 times cheaper than individual RE elements.

AIM OF PROJECT WORK:

In the present work an effort has been made to develop a new Mg-alloy system that possesses exceptionally high ductility as well as good mechanical strength. Mg based alloys have been developed to find out considerable ductility, elongation, strength, Hardness, wear characteristics, microstructure and phase identification at room temperature in as-cast state. Misch metal is added in Mg-based alloys to investigate the changes in mechanical properties. Reports on the effect of MM on the as cast microstructure and mechanical properties are important.

Based on above objectives, the entire thesis is classified into five chapters. The introduction of the present investigation including the objectives of the work is described in this chapter. The brief literature review related to the present investigation is presented in Chapter-2. Chapter-3 contains the experimental procedure of the work. Studies on evolution of microstructure and mechanical properties of Mg-Al-Zn-Sn-Pb based alloys have been presented in Chapter-4. The tribological behaviour of Mg-Al-Zn-Sn-Pb based alloys is reported in Chapter-5. The major conclusions that derived from the work are given in Chapter-6.

2.1 Introduction:

One of the paramount considerations of automotive manufacturers is to reduce to the weight of passenger car. This effort will not only reduce the fuel consumption but also reduce the burden on the environment leading to minimize the green house effect. Unfortunately, the weight of passenger car has gained the weight more than 20% in last 20 years. The principal causes of such increase in weight are the additional safety features of the passengers and increased average engine size. However, the customer's consciousness of fuel efficiency has triggered by increasing fuel prices and the concern of environmental issues. Thus, weight reduction is an essential mission for automobile producers. "Concept cars" produced in recent years have been lightweight, for example, the 'Ford P2000' (weighs only 544.3 kg) [4], which reduces emission levels dramatically and improved engine efficiency. The weight reductions have been made possible by the replacement of steel by light metal alloys, usually Al-alloys or Mg-alloys or by fibers. Earlier, Al-alloys replaced most of steel or cast iron components in automobiles. At present, the main endeavor and assignment of the researchers is to find appropriate material, which is more efficient than Al so as to reduce the weight of automobile a maximum possible further extent. Magnesium and its alloys are one such potential material, whose light-weight advantage could be used for wide range of applications including automobile structural materials. Magnesium, with a density of 1.7 g/cc is the lightest of the structural materials. It is two third of its counterpart aluminum (density: 2.7 g/cc) and one third of steel (density: 7.8 g/cc). It has high specific strength properties over aluminum alloys. But, unfortunately the total annual

Consumption of Mg (~250 thousand tones) is a fraction of Al (20 million tons) used throughout the world. The last decade has seen a growth in Mg- castings for the light vehicles ~16% per year and is predicted to grow at an annual rate of ~11.5% for the next decade. Even then, it is believed that Mg is not being utilized as it should be. This is mainly due to the fact that the metallurgical knowledge of Mg and its alloys is immature compared to that of Al and its alloys. Therefore, a wide scope of research exists in Mg- based alloys.

Both Al and Mg metals were discovered in the early 19th century and industrial refining processes for each metal were announced in 1886. But the lower consumption of Mg is due to different complex of factors. However, developments in magnesium refining and processing technology have coincided with new demands from many industries for high precision light-weight die-castings. Now the use of magnesium is growing at a faster rate than any other metal. While there is no doubt that the maximum user of magnesium in tonnage terms is the automotive industry, there are newer 'High-Tech' industries, which are beneficially exploiting the properties of magnesium die-casting. While the light weight is certainly the major reason for the renewed interest in magnesium castings, there are a number of other properties, which make magnesium a preferred choice for components in industrial applications. Table 2.1 compares some of the typical physical properties of magnesium alloy (AZ91), aluminum alloy (LM 24) and glass-reinforced plastics molding material [5].

Table 2.1

Comparison of various properties of Mg-alloy with Al-alloy and plastic [5]

Properties	Magnesium alloy(AZ91)	Aluminum alloy (LM24)	Plastic Lexan 3413
Yield strength(MPa)	160	150	N/A
Tensile strength (MPa)	230	320	130
Elongation (%)	0.5-3	1-3	3-5
Shear strength (MPa)	140	185	72
Elastic modulus (GPa)	45	71	8.6
Density (g/cc)	1.81	2.79	1.43
Specific heat (J/kg/ºK)	1050	963	0.27
Expansion coefficient(x10-4 /ºK)	26	22	22
Thermal conductivity(W/MºK)	72	96	0.21
Electrical conductivity(%IACS)	11.2	24	Nil

2.2 Magnesium's Characteristic Profile

Mg is mainly extracted by Pidgeon process from its carbonate compound and is readily available commercially with purities > 99.8%. It has hexagonal crystal structure with c:a ratio of 1.6236 very close to the ideal value of 1.633 for the atomic packing of spheres [6]. The atomic diameter of Mg is 0.320 nm. Fig. 2.1 shows the schematic planes and directions in the Mg unit cell. Though at room temperature Mg has only three active slip systems, all parallel to the basal plane (0001) [2], at higher temperature, both prismatic and pyramidal slip planes are also become active leading to the work hardening.

2.3 Magnesium based alloy systems

A number of alloying elements are present in various commercial Mg-alloys. The solubility data for binary Mg-alloys are shown in Table 2.2. A wide range of intermetallic compounds may form in Mg alloys. Among these compounds the following three types of structure are most common.

(i) AB type: Simple cubic CsCl-type structure. e.g., MgAg, MgCe, SnMg.

(ii) AB_2 type: Laves phases with ratio RA/RB = 1.23. e.g., $MgCu_2$ (fcc), $MgZn_2$

(iii) CaF_2 type (fcc): Mg_2Si, Mg_2Sn

Table 2.2

Solubility data for binary Mg-alloys

Element	at.%	wt. %	System
Aluminium	11.8	12.7	Eutectic
Lithium	17	5.5	Eutectic
Silver	3.8	15.0	Eutectic
Yttrium	3.75	12.5	Eutectic
Zinc	2.4	6.2	Eutectic
Neodymium	0.98	3	Eutectic
Zirconium	1	3.8	Peritectic
Manganese	1	2.2	Peritectic
Cerium	0.1	0.5	Eutectic
Cadmium	100	100	Complete S.S
Scandium	15	24.5	Peritectic
Lead	7.75	41.9	Eutectic
Tin	3.35	14.5	Eutectic
Silicon	0.003	0.8	Eutectic

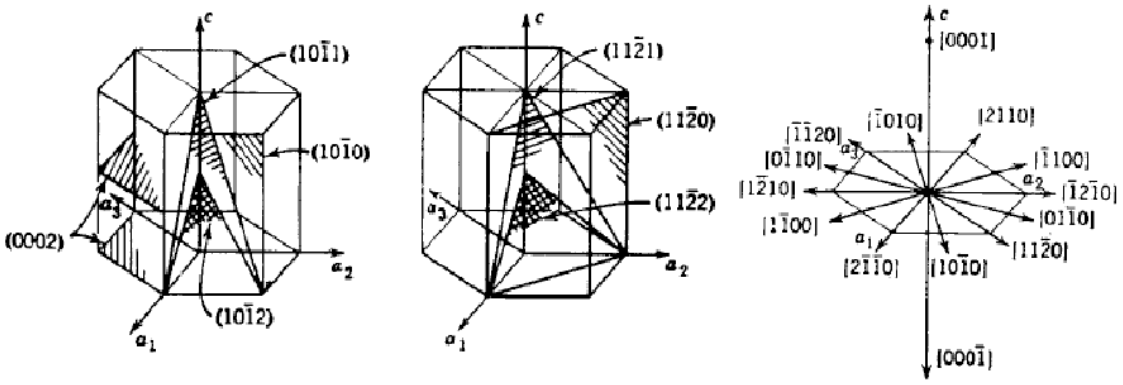

Fig. 2.1 Principal planes and directions in the Mg unit cell [6]

Al is the most common alloying elements in Mg alloys. The major commercial Mg alloys along with their compositions are shown in Table 2.3 [7]. AZ91 alloy (9%Al - 1%Zn - 0.2%Mn) is mostly used in automotive industries. The alloy provides very good room temperature tensile properties, excellent casting properties and corrosion resistance [8]. Al in AZ91 alloy offer better castability, strength and corrosion properties. Zn improves the solid solution strengthening whereas Mn provides corrosion resistance. Therefore, 90% of Mg alloy components used in transport industries are made from AZ91 alloy [9]. However, AZ91 alloy does not exhibit good creep resistance which is a major setback [10]. The mechanical properties of some of the die cast Mg alloys are given in Table 2.4 [11].

Table 2.3

Major compositions of some of the Mg-Al based alloys [7]

Alloy	Al	Zn	Si	Mn	RE	Cu	Fe	Ni	Mg
AM20	1.7-2.2	<0.1	<0.1	>0.5	….	<0.008	<0.004	<0.001	Rest
AM50	4.5-6.3	<0.1	<0.1	>0.27	….	<0.008	<0.004	<0.001	Rest
AM60	5.7-6.3	<0.2	<0.05	>0.27	….	<0.008	<0.004	<0.001	Rest
AS41	3.7-4.8	<0.1	0.6-1.4	0.22-0.48	…	<0.04	….	<0.01	Rest
AZ91	8.5-9.5	0.45-0.9	<0.05	>0.17	…	<0.015	<0.004	<0.001	Rest
AE42	3.6-4.4	<0.2	…	>0.27	2.0-3.0	<0.04	<0.004	<0.004	Rest

Table 2.4

Mechanical properties of different Mg-Al based alloys [11]

Alloy	Condition	Yield Strength(Mpa)	Tensile strength(Mpa)	Elongation(%)
AZ91	Die Cast	150	230	3
AM60	Die Cast	115	205	6
AS41	Die Cast	150	220	4
AS21	Die Cast	130	240	9
AE41	Die Cast	103	234	15

2.3.1 Magnesium alloy designation and major alloy systems:

No international code for designating Mg alloys exists although there has been a trend towards adopting the method used by the American Society for Testing Materials (ASTM). In this system, the first two letters indicate the principal alloying elements according to the following code. The code has shown below in table 2.5.

Table 2.5

Coding for Magnesium based alloys

Abbreviation letter	Alloying element	Abbreviation letter	Alloying element
A	Aluminium	P	Lead
C	Copper	Q	Silver
D	Cadmium	R	Chromium
E	Rare earth	S	Silicon
F	Iron	T	Tin
H	Thorium	Z	Zinc
K	Zirconium	M	Manganese

2.3.2 Zirconium free alloys (Mg-Al Alloys):

Aluminium is the principal alloying element in Mg. Its alloys containing 8-9% Al and small amount of Zn are widely used for various applications. AZ91 and AM50 are most widely used alloys in these groups [12]. These alloys have a wide range of mechanical properties and good castability, and mostly used in die casting application. Small amount of Mn is added to improve corrosion resistance. The drawback of using these alloys is its poor elevated temperature tensile and creep properties above 150^{o}C [10]. Mg-Al alloys containing Si (e.g., AS21, AS41) are developed for better creep properties compared to AZ91 [13]. The solubility of rare earth in Mg which is 1.6 wt.% at 590ºC led to the development of AE alloys systems.

2.3.3 Zirconium containing alloys:

The maximum solubility of Zr in molten Mg is 0.6% [14] as shown in Fig. 2.2. The binary Mg-Zr alloys are not sufficiently strong for commercial applications, so the addition of other elements is necessary. The selections of these elements are governed by mainly, compatibility with Zr, founding characteristics and required properties. The ability to grain refine Mg-Zn alloys with Zr led to the introduction of ternary alloys such as ZK51 (Mg-4.5Zn-0.7Zr) and higher strength ZK61 (Mg-6Zn-0.7Zr) which are normally used in T5 and T6 tempers, respectively. However, these alloys are susceptible to micro-porosity and are not weldable, which limited their practical applications [12]. This micro-porosity can be minimized by the addition of rare earth elements or cheaper misch metal (comprising Ce, La, Nd, Pr etc) which

form low melting point eutectic and form a network along the grain boundaries. The addition of misch metal to Mg gives good casting characteristics and excellent mechanical properties. These properties could be improved by adding Zr to refine grain size. Addition of Zn further improves the mechanical properties. EZ33 (Mg-3RE-2.5Zn-0.6Zr) is one such alloy, which retains strength and creep resistance at temperatures up to 250^{o}C [15]. Series of Mg-Y-Nd-Zr alloys have been produced, which provides high strength at ambient temperature and good creep resistance up to 300^{o}C temperature [16, 17]. Mg alloy containing Y and Nd, e.g., WE54 (Mg-5.25Y-3.5RE-0.45Zr) gives excellent strength combined with good ductility. Ag is also added to Mg and Mg-Ag-RE-Zr alloys are developed with improved room and high temperature mechanical properties [18]. The alloy QE22 (Mg-2.5Ag-2RE-0.7Zr) has been used in aerospace applications including landing wheels, gear box housings and rotor heads for helicopters. These applications showed Mg-alloys have the potential for automotive and aerospace industry.

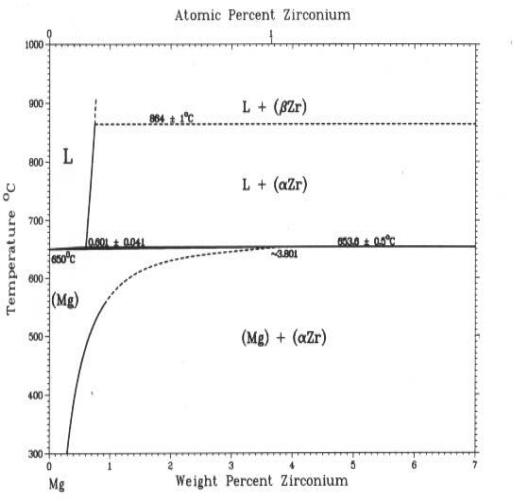

Fig. 2.2 Phase diagram of Mg-Zr binary alloy [14]

2.4 Effect of alloying elements:

Since the beginning of the demand of Mg-alloys researchers are putting their effort to improve the properties of pure Mg with different alloying elements. The main mechanism for improving the mechanical properties is precipitation hardening and/or solid-solution hardening. While solid-solution hardening is determined by the differences in the atomic radii of the elements involved, the effectiveness of precipitation hardening mainly depends on a reduced solubility at low temperatures, the magnesium content of the intermetallic phase, and its stability at application temperature. Magnesium forms intermetallic phases with most alloying elements, the stability of the phase increasing with the electro negativity of the other element. By the 1920s, aluminium had already become the most important alloying element for significantly increasing the tensile strength, specifically by forming the intermetallic phase $Mg_{17}Al_{12}$. Similar effects can be achieved with zinc and manganese, while the addition of silver leads to improved high-temperature strength. High percentages of silicon reduce the castability and lead to brittleness, whereas the inclusion of zirconium forms oxides due to its affinity for oxygen, which are active as structure-forming nuclei. Because of this, the physical properties are enhanced by fine grain hardening. The use of rare earth elements (e.g. Y, Nd, Ce) has become more and more popular since they impart a significant increase in strength through precipitation hardening. For example, the mechanical properties of Mg-4Al-2RE (AE42) alloy are greatly improved due to formation of highly thermal stable precipitates and complete suppression of β $Mg_{17}Al_{12}$ phase[19,27]. All these

elements increase susceptibility to corrosion, as established by the precipitation of cathodic compounds when they solidify. In contrast to regular cases, where a magnesium oxide or hydride layer protects the metal and lowers corrosion rate, these elements increase the corrosion rate. This is one of the reasons why alloy development has been directed towards “high-purity” (HP) alloys with very little use of iron, nickel, or copper.

2.4.1 Common Alloying Elements

2.4.1.1 Aluminum

Aluminum is the most commonly used alloying element and forms the basis of the die casting alloys. The maximum solubility is 11.5 at % (12.7 wt %) and alloys in excess of 6 wt % can be heat treated [20]. Aluminum improves strength, the optimum combination of strength and ductility being observed at about 6%.Alloys is readily castable. The creep resistance is limited due to the poor thermal stability of the $Mg_{17}Al_{12}$ phase. The Mg-Al binary system is origin of some of the oldest and most commonly used casting alloys. Alloys such as AZ91, AM50, and AM60 still comprise a large portion of all magnesium alloy casting. Figure 2.3 shows the Mg-Al phase diagram .The maximum solubility of Al in Mg ranges from about 2.1wt% at 25°C to 12.6wt% at the eutectic temperature of 437°C. The eutectic composition is 32.3wt% and the eutectic is between a-Mg and the ß-phase, which is $Mg_{17}Al_{12}$. The effect of Al addition on the tensile properties of Mg-Al alloys are illustrated in Fig. 2.4 [21].

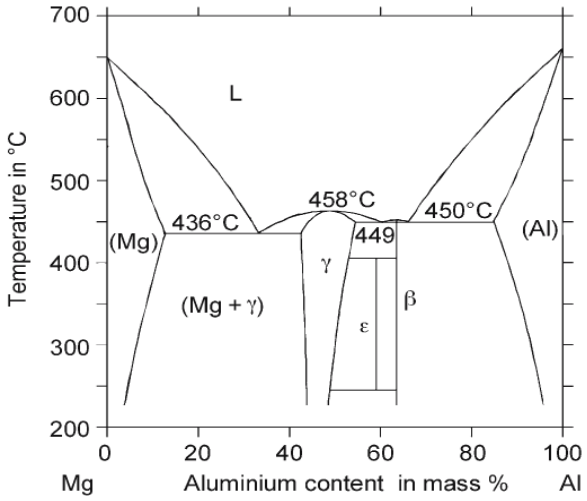

Fig. 2.3 Phase diagram of Mg-Al binary alloy [20].

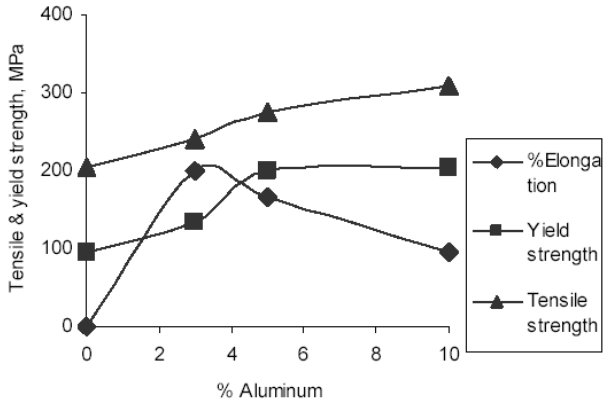

Fig. 2.4 Effect of aluminum on the mechanical properties of Mg-Al binary alloy [21]

As expected from the phase diagram, Mg-Al alloys are precipitation heat treatable, although solutionizing and aging of Mg-Al alloys do not have the effectiveness seen in many Al-Si alloys as the ß- $Mg_{17}Al_{12}$ precipitate forms in an incoherent manner. Mg-Al binary alloys are generally highly castable and typically have good mechanical properties.

However, commercial alloys are rarely binary alloys; they are mostly ternary and quaternary alloys with additions of zinc, manganese, rare earth metals, and silicon, they also complicate the solidification behavior of the alloy.

2.4.1.2 Zinc

Zinc is one of the commonest alloying additions. It is used in conjunction with Al (e.g., AZ91 or with zirconium, thorium or rare earths). Zinc is an important alloying element but rarely serves as the major alloying element (ZK, ZH, ZM, ZC and ZE series of alloys). The binary phase diagram of Mg-Zn (Fig. 2.5) shows a eutectic at 51.3 wt % [22].

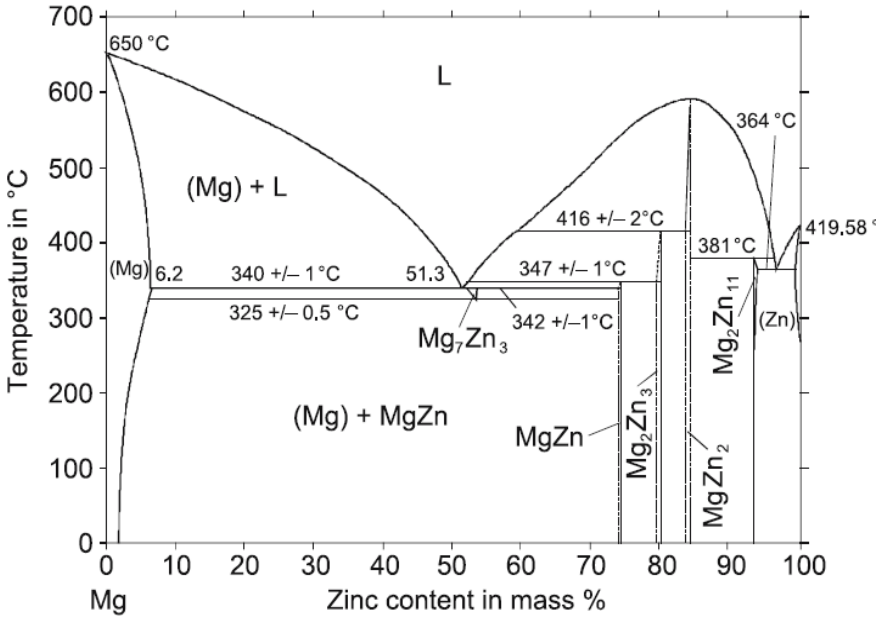

Fig. 2.5 Phase diagram of Mg-Zn binary alloy [22].

2.4.1.3 Tin

Small amounts of Sn, in conjunction with small amounts of Al, serve to improve ductility and reduce the tendency to cracking during forging. It, thus, becomes apparent how few elements are responsible for producing the desired properties. The mechanical properties of Mg-alloys are significantly improved by addition alloying elements. Sn as an alloying element can increase the strength by solid solution strengthening [23]. Additionally, the solubility of Sn in α-Mg drop sharply decreases with decreasing temperature, which can further improve the mechanical properties through aging. Meanwhile, the Mg_2Sn precipitate (face-centered cubic structure) in Mg-Sn binary alloy has a high melting temperature, which can effectively hinder dislocation and grain boundary sliding. The binary alloy phase diagram of Mg-Sn is represented in Fig 2.6. Two eutectic reactions and a congruently melting line compound, Mg_2Sn, characterize the Mg-Sn system. The maximum solid solubility of Sn in Mg is 14.48 wt% at 561.2ºC [23].

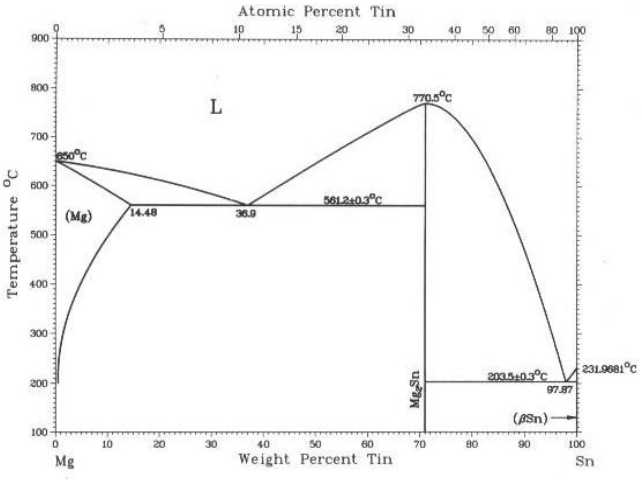

Fig. 2.6 Phase diagram of Mg-Sn binary alloy [23]

2.4.1.4 Silver

Silver increases the age hardening response and high temperature properties of thorium or rare earth containing alloys. The binary phase diagram of Mg-Ag (Fig.2.7) shows a eutectic at 48.1 wt % at 473ºC. There is 15.3 wt % at 472ºC solubility at the eutectic temperature.

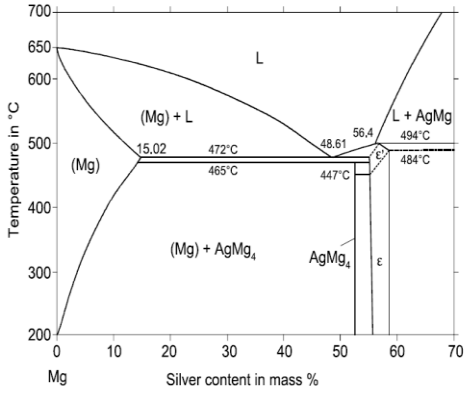

Fig. 2.7 Phase diagram of Mg-Ag binary alloy [24]

2.4.1.5 Silicon

Silicon increases the fluidity of molten alloys. In the presence of Fe it will reduce the corrosion resistance. It is employed in very few alloys (AS21 and AS41). Figure 2.8 shows the Mg-Si phase diagram.

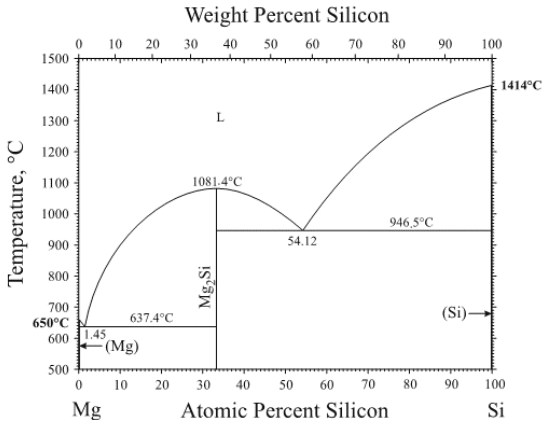

Fig. 2.8 Phase diagram of Mg-Si binary alloy [25]

2.4.1.6 Lead

Lead has a relatively high solubility to Mg matrix (41.7 wt. % at the eutectic temperature and 5 wt. % at 200ºC) as shown in Fig. 2.9 , and therefore, may provide good solid-solution strengthening effects to the Mg alloys. It is also suggested that the solid solution of Pb can improve the ductility of Mg matrix by modifying the dislocation movement system [18], although the detailed mechanisms are not clear. Lead atoms in the Mg matrix may slowdown the diffusion rate of alloying elements in Mg, therefore affecting the formation and reducing the amount of intermetallics in Mg alloys.

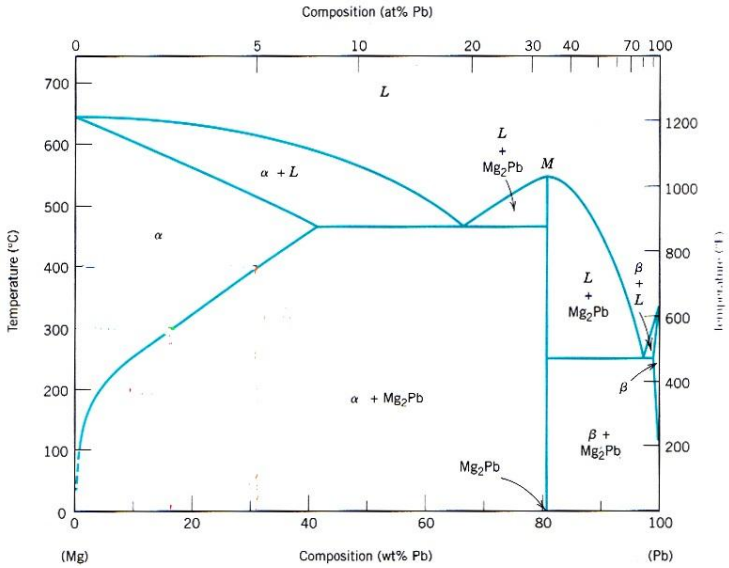

Fig. 2.9 Phase diagram of Mg-Pb binary alloy [26].

2.5 Melting Practice

During melting of Mg-alloys utmost care must be taken to shield the molten metal surface against oxidation. Molten Al-alloys tend to form a continuous, impervious oxide skin on the molten bath and thus, limits further oxidation but Mg-alloys behave differently. Mg-alloys form a loose, permeable oxide skin on the molten metal surface. Due to pervious oxide layer, oxygen passes easily through this layer and burns the entire melt. The reasons behind the burning of Mg-alloys are as follows:

The oxidation of Mg during melting process are normally eliminated by using fluxes, e.g., melting and refining fluxes. The melting flux normally consists of chlorides and fluorides ($MgCl_2$, KCl, NaCl, CaF_2, etc.). The liquidus temperature of the melting flux must be below the solidus temperature of the alloy to be melted. The flux should have sufficient fluidity and wetting power so that it can easily spread out on the melt to form a completely protective layer over the melt. In the molten metal of Mg many nonmetallic inclusions suspend. These inclusions would enter into the casting and reduces the casting quality unless these are removed before pouring [28]. An “inspissated” flux (refining flux) is used for this purpose. “Refining process” is a method where oxides are removed by inspissated flux. A fresh cover of inspissated flux is applied to the metal surface and the melt is vigorously stirred with a rotary motion for 1-2 minutes. After stirring, the metal surface is covered with a thick layer of the flux which quickly melts and after a few minutes it forms a coherent viscous cake. This excludes air effectively, so long as the metal is undisturbed and can readily be drawn away from the crucible lip before casting. [28, 29]. $MgCl_2$ is the

essential constituent of the inspissated flux. In flux-less melting inert gases are used to protect the molten metal against oxidation. SF_6 mixed with dry air and CO_2 is the most common gas used in the flux-less melting [30].

2.6 Processing of alloys

2.6.1 Conventional casting

Generally, the magnesium alloys are cast by die casting method. This is to overcome the material cost disadvantages compared to aluminium alloys [31]. Thus, all Mg- alloys development activities for different mechanical properties are focused with die-castability [32]. Magnesium alloy containing Al as a major alloying element has high die castability compared to other Mg alloys. The most commercial and widely applied die cast magnesium alloys are AZ91, AM60, and AE42 etc. The choice of a particular casting method depends upon many factors, e.g., the number of castings required, the properties required, dimensions and shape of the part and the castabiltiy of the alloy. Although pressure die casting is predominantly used to produce many of the magnesium alloy components, other casting processes such as gravity and low pressure castings using sand and permanent moulds are also familiar. Mg-Al and Mg-Al-Zn alloys are also easy to cast in gravity sand casting method; however they are limited in certain respects. They exhibit micro shrinkage when they are sand-cast, and the alloy is not suitable for applications in temperatures of above 120°C. Magnesium alloys containing rare earth as a major alloying element are mainly produced in sand casting route and they are used in aerospace applications.

2.7 Heat Treatment

Heat treatment schedule plays a major role in achieving a desired microstructure and mechanical properties of Mg-based alloys. In Al-containing Mg-based alloys due to the wide range of solubility of Al in Mg, $Mg_{17}Al_{12}$ phase precipitates during its solidification and during ageing treatment which is responsible for appropriate mechanical properties [33].

2.8 Mechanical Properties

Properties of Mg alloys are depended on its microstructure, grain size, volume and size of second phase etc [34,35]. Porosity and interdendritic shrinkage are also play a major role to determine the mechanical properties of the alloy [36]. The mechanical properties are also sensitive to temperature, strain rate and other test conditions.

2.8.1 Effect of temperature and strain rate

$Mg_{17}Al_{12}$ intermetallic, in AZ91 alloy, is responsible for room temperature strengthening effect. This intermetallic has low melting point (437^{o}C) and has a tendency to become coarsen at elevated temperature (>100^{o}C) and no longer act as a barrier for dislocations [37]. Moreover, $Mg_{17}Al_{12}$ intermetallic is incoherent with the hcp Mg matrix because of its cubic crystal structure. Therefore, in AZ91 alloy this phase leads to the poor elevated temperature properties. It should be noted that temperature has a great effect on the tensile properties at lower strain rate whereas at higher strain rate, the temperature effect is less significant [38].

2.8.2 Effect of grain size

Mechanical properties are highly dependent on grain size. The yield strength can be related with grain size by well-known Hall-Petch equation;

$$\sigma_{=} \sigma_{o} + Kd^{-1/2}$$

where σ_o is the yield stress of a single crystal, *K* is a constant and *d* is the grain size and σ is the yield stress. With increasing the Taylor factor the value of *K* increases [39]. On the number of the slip systems the Taylor factor is generally depended. Because the Tailor factor is larger for HCP metal and the slip systems are limited as compared to FCC and BCC metals, HCP metals exhibit the strong influence of grain size on strength [40]. Both strength and ductility are improved with reduction in grain size. By thermo- mechanical treatment and severe plastic deformation the higher strength and ductility are obtained. This is due to the fact that these processes provide fine grain size in the order of 1μm. It is observed that intergranular fracture is occurred in Mg alloy with a large grain size: however, intergranular fracture is limited in Mg alloy with a small grain size [41], indicating that the fracture mechanism is changed by grain refinement. This is because the critical stress for crack propagation at grain boundaries increases with decreasing grain size [41].

2.9 Wear Behavior

Wear of metals is probably the most important yet least understands aspect of tribology. Wear, in the broadest sense, may be defined as the removal of surface material of a component. Wear of machine parts means replacement and this by itself expensive. Moreover, worn-out surfaces cause a loss of precision with the resultant sacrifice in efficiency. Therefore, it is required to design the machine parts for a minimum amount of wear. Friction and wear are not the intrinsic material properties. They are dependent on both the working conditions and the properties of materials. Widely varied wearing conditions cause wear of materials by various mechanisms. Small changes of load, speed, frictional temperature or properties of materials including microstructures cause remarkable changes in the wear of contact surfaces. Wear properties are important especially when Mg alloys are to be applied for critical automobile applications. There are several mechanisms of wear, which include seizure, melting, oxidation, adhesion, abrasion, delamination, fatigue, frettling, corrosion, and erosion [42, 43]. Wear may normally be reduced by using a lubricant with appropriate anti-wear additives or changing the materials and/or the operation parameters affecting the wear rate. Chen et al. [44] have carried out a dry sliding wear testing on AZ91 alloy against AISI 52100 steel ring within a load range of 1-350 N and a sliding velocity range of 0.1 - 2 m/s. They observed two main wear regimes, namely a mild wear regime and a severe wear regime. In the mild wear regimes, it is found that the volume loss due to sliding wear increased linearly with the sliding distance whereas in the severe wear regimes, it is no longer linear. Oxidation wear and delamination wear are reported in mild wear regime.

2.10 Applications

Magnesium is employed extensively in aircraft engines, air frames and landing wheels [45]. Alloys such as ZE41 (Mg-4.2%Zn-0.7% Zr-1.3% MM), QE22 (Mg-0.7% Zr-2.5% Nd-2.5% Ag) and particularly WE43 (Mg-4% Y-3.25% Nd-0.5% Zr) are commonly used for aircraft applications due to their improved corrosion and creep resistance. High specific strength and rigidity coupled with ease of fabrication are important for missile and space applications. EZ33 (Mg-2.7% Zn-0.7% Zr-3.2% MM) sand castings are used in the “Skylark” research rockets. Automobile industries are the latest beneficiary of magnesium, currently exploring its maximum usage. Steering wheel, cylinder head cover, door frames, transmission housing, structural supports are the potential specific application areas in automotive industry [46]. Mg can be used in nuclear industry as it has low tendency to absorb neutrons, does not alloy with uranium and adequate resistance to carbon dioxide up to the highest service temperatures envisioned. Apart from transport and missile components Mg also finds application in electronics and house holding items [47].

2.11 Limitations

In spite of several advantages and applications of Mg-based alloys, there are some limitations which restrict its full utilization for industry applications. Some of the challenges that are facing magnesium in order for its wholesale acceptance for industrial applications are high metal cost, high cost of recycling, lack of joining techniques and poor workability.

Materials and experimental details:

In this section, the experimental set-ups used for the work are briefly described. During the experiments, some of the conventional set-ups were used, and some of the set-ups were rectified according to the experimental need. The entire experimental work comprised the following steps.

3.1 Materials:

3.1.1 Metals and master alloys:

Mg-Al-Zn-Sn-Pb based alloys have been selected for the present study. These alloys were prepared through melting process using Mg ingots (purity: 99.85%), Sn granules (purity: 99.99%), Al ingots (purity: 99.96%), Zn flake (purity: 99.99%) ,Si granules (purity: 99.999%) Pb granules (purity: 99.999%), Misch metal (purity: 99.999%). The alloy compositions are shown in Table 3.1.

3.1.2 Crucible:

For the melting of Mg-alloys a mild steel crucible of capacity ~ 3 kg was used. The melting was done within a resistance heating furnace with the provision of maintaining controlled atmosphere. In order to remove the oxides sticking on the wall and bottom of the crucible from the previous melting the crucible was filled with water and kept for one day for oxides to get dissolved. Then, it was cleaned with mild steel wire brush.

3.1.3 Melting and refining flux:

Selection of flux is an important consideration for melting of Mg-alloys. In the present experiment the flux *'Magrex-60'* a trade product of '*FOSICO'* industries, was used for covering and refining the molten metal during melting. $MgCl_2$, MgF_2, MgO etc. are the major composition of the flux. Fine sulfur powder was also used for dusting around the melt jet to remove the oxygen so as to avoid oxidization during pouring of molten metal into the mould.

3.1.4 Mould:

Two cast iron rectangular and cylindrical moulds were used throughout the experiments. In order to avoid the spilling of molten metal a pouring basin was attached to the sprue of the mould. The mould set up was preheated to 250 ^oC in order to avoid the chances of partial solidification in the sprue area. A stainless steel mesh was used at the top of the pouring basin to reduce the oxide inclusions in the casting. Cast iron mould of dimension (250x80x20 mm^3) shown in Figure 3.1 was used throughout the experiments.

Figure 3.1 Schematic diagram of the mould used for magnesium alloy castings

3.2 Melting and pouring:

3.2.1 Melting:

The melting arrangement for Mg alloys is presented in Fig. 3.2. All the tools and metal ingots were preheated before use. The preheated flux was sprinkled in the bottom and at the sides of the cleaned crucible and kept inside the furnace. The furnace temperature was raised to the predetermined temperature and argon gas (purity 99.999%) was passed. After the crucible reached the red hot condition, the preheated ingots were charged in to the crucible. Initially, part of the total Mg ingots was charged. After the melting of charged ingots, the remaining ingots were then immersed into the molten metal. This kind of charging practice of metal ingots avoids the excessive oxidation during melting. Crucible was covered with furnace lid to minimize the air contact with the molten metal. Flux was sprinkled over the metal throughout the melting. Before addition of alloying elements, the top layer of oxides was completely removed with a skim ladle and fresh layer of flux was applied. The required amounts of master alloys were weighed and were slowly immersed into the melt. After additions, the melt was gently stirred for dissolution of the added elements. Again the top oxide layer was removed and fresh layer of flux was applied. The melt at a temperature of about 720-750 ^{o}C was held for 30 minutes to ensure the complete dissolution of elements in the melt.

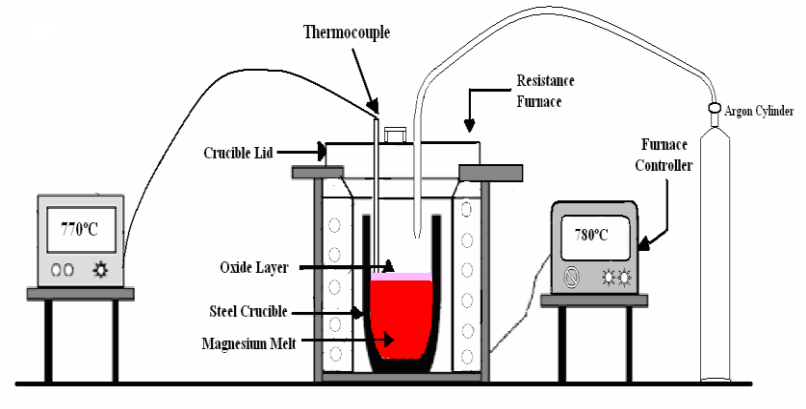

Fig. 3.2 Schematic diagram of the melting arrangement for Mg-based alloys

Fig. 3.3 Melting arrangement facility of developed Mg-alloys at CSIR-NML

3.2.2 Pouring and Casting:

The molten metal was poured into the preheated mould after refining operation. During pouring care has been taken to avoid the breakage of top flux protective layer. The pouring was carried out gently without any jerk in the melt, since excessive jerk disturbs the settled oxide inclusions in the bottom. The flux layer near the lip of the crucible was pulled back gently by using a skimmer for smooth flow of molten metal. Sulfur powder dusting was carried out to remove the oxygen around the melt jet. Fig 3.4 shows the flow diagrams of Mg-based alloys.

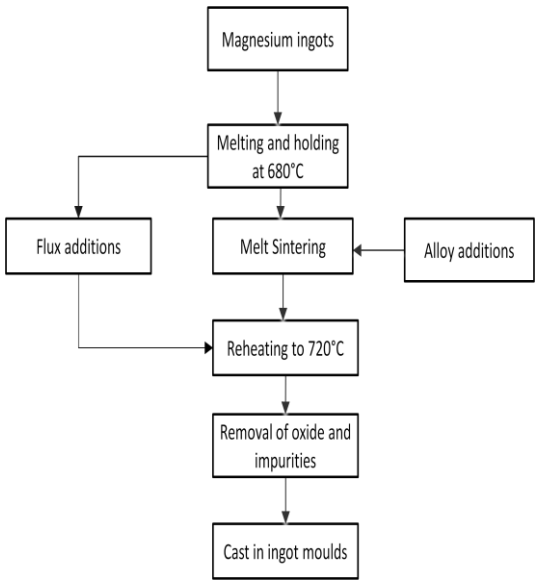

Fig. 3.4 Flow chart showing processing sequence for the developed Mg alloys

Table 3.1

Different alloys prepared for the present study

Alloy Designation	Alloy composition
H1	Mg-4Al-3Zn-3Sn-3Pb
H2	Mg-4Al-3Zn-3Sn-3Pb-0.5MM
H3	Mg-3Zn-3Sn-3Pb-2Si

Where MM= Misch Metal (Purity; 52%Ce-26%La-16%Nd-6%Pr)

3.3 Heat treatment:

3.3.1 Solution treatment:

Solution treatment was carried out in order to homogenize the alloys. A sand bed prepared using carbon charcoal and dry silica sand with a volume ratio of 25:75 was placed in the muffle furnace. Samples were placed in a mild steel tray in such way that no piece touches others. The charcoal-silica sand mixture was also put in the tray burying the samples. This helped to evacuate oxygen present in the furnace during heat treatment. This procedure was found satisfactory to avoid the oxidation of magnesium samples during the heat treatment. The samples were solution heat treated for 8-10 h followed by immediate water quenching at room temperature.

3.4. Hardness:

The vicker's hardness tester (Model-UH3, Reicherter, Stiefelmayer) was used for the measurement of hardness in as cast and heat treated samples. Before the hardness measurement the sample was polished up to 800 grit fine emery paper to remove the oxide and other scales for clear observation of indentation mark. Diamond pyramid indenter was used to make indentation. Load was fixed at 1 kg with a dwell time of 10 s. The micro hardness measurement on the sample was done using a LECO micro hardness tester (Model Leica-VMHT, Germany) under a load of 50 g. Micro hardness measurements were taken at several places of the sample. The hardness value of each indentation was calculated by the machine using the following relation:

$$H = P_{max}/A = (2P\sin\theta/2) / L^2 = 1.854\, P_{max} / L^2 \quad \text{.....3.1}$$

where, P_{max} is the applied load, A is the area, L is the average length of indentation, θ is the angle between opposite faces of diamond pyramid (136°), and H is the hardness. Ten readings for each sample were taken and its average has been reported as the hardness value of that particular sample.

3.5 Microstructural observation:

3.5.1 Sample preparation:

The microstructure and properties of the samples varied along the surface to center portion of the casting. Therefore, in order to maintain the uniformity in microstructure, all the samples were taken from the central region of the castings.

3.5.1.1 Polishing:

The samples were polished using different grade of emery paper with progressively coarse to finer one (320, 400, 600, 800, 1000, 1200, 2000 grits). After completing the paper polishing, the samples were polished in a rotating disc of proprietary cloth with silica suspension. Since Mg is a soft material care was taken during polishing to avoid scratches and excessive surface contamination. Finally, the samples were cleaned using ethanol as the cleaning with water was not sufficient to remove surface contaminants. The grain structure was revealed by subsequent etching using a solution of ethanol (100 ml), picric acid (5 g), acetic acid (5 ml), and water (10 ml). After chemical etching, a residual layer remained in the sample surface that was eliminated by immersion in ethanol.

3.5.2 Optical microscopy (OM)

A LECO, a trade name of Leco Corporation, MI optical microscope equipped with image analysis software, a camera and a computer was used for the OM observation and the quantitative measurements of micro structural features. A software application was used to acquire images from the camera and to perform image analysis.

3.5.3 Image analysis:

The volume fraction of precipitate phase and grain size of the alloy/composite in selected samples were estimated with the help of an image analysier (LECO, a trade name of Leco corporation, MI). In each case, at least sixteen fields were analyzed from a single specimen and the average value is reported.

3.5.4 Electron probe micro-analyzer (EPMA):

Electron Probe Micro Analyser (EPMA) of make JXA-8230, JEOL, Japan, was used phase analysis of some of the samples. It can analyse elements both qualitative and quantitatively. Depending on requirement W and LaB6 filament can be used. Point, line and area analyses are possible, also elemental distribution can be identified by map analysis. The minimum probe size is 0.5 micron.

3.5.5 Field emission gun scanning electron microscope (FEG-SEM):

Field Emission Gun Scanning electron microscopes (FEG-SEM) was used for microstructural characterization of the samples. Fracture surface of the tensile samples as well as the worn out surfaces of the wear testing surfaces was also observed under FEG-SEM.

3.6 X-ray diffraction (XRD):

The types of different phases in a sample were identified using XRD. 15 mm diameter and 3 mm thick samples were cut from the castings and the surface scales were removed by rough polishing. XRD spectrums were obtained using BRUKER D8 DISCOVER Powder diffractometer with Cu-K_α radiation (λ= 1.5418 Å). The samples were polished and cleaned before subjecting to diffraction studies. X-ray diffraction pattern for each of the samples were taken for 2θ values ranging from 20-90º. Scanning speed was 2º/min. The peak position was identified from the graph and corresponding 2θ values were noted. From the 2θvalues, planner spacing (d) were calculated using the Bragg's law of diffraction. The d (planner spacing) was matched with standard x-ray diffraction files and phases were identified.

3.7 Density measurement:

Change in density of metal during solidification results in shrinkage of casting. It is also influenced by the nonmetallic inclusions and gas porosity. Thus, the observation of the density variation in the casting can give a clue to the distribution of the fibers and the porosity. Archimedes water displacement method was used for density measurements. In order to observe the density variation along the length of the casting, 5 samples were taken from the casting along the length than specimens were weighed in air and then in water. The measurement was carried out with the help of electronic balance. The weight in air divided by the loss of weight in water gives the density of the specimen.

3.8 Mechanical properties:

3.8.1 Tensile testing:

The tensile testing was carried out using computer controlled INSTRON 8501 Universal Testing Machine and MTS 810 Material test system at room temperature (25^0C). Samples for tensile testing were prepared according to ASTM E8M standard. Ultimate tensile strength (UTS), yield strength (YS) and elongation were recorded. For room temperature test extensometer was used to get the percentage of elongation during testing, also the ductility was measured manually after the test. Two tensile samples was made from the each of the casting alloys. The average of two sample testing data was reported. Fig. 3.5 shows the schematic diagram of the tensile specimens for room temperature (25ºC) tensile testing.

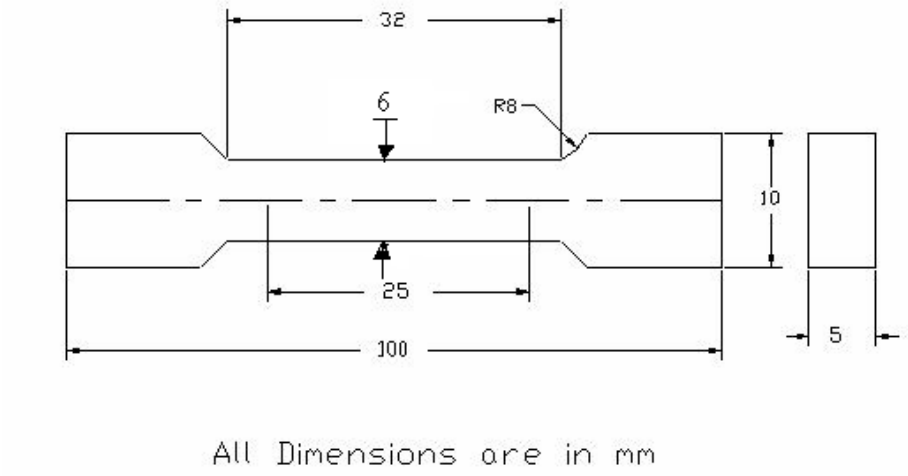

Fig. 3.5 Schematic diagram of a tensile specimen (ASTM E8 Standard) tested at room temperature.

3.9 Wear Testing:

The sliding test wear carried out using pin-on-disc machine (model TR 20, manufactured by Ducom, Bangalore, India). Pin of 6 mm diameter wear made to slide against a low alloy steel disc of hardness 62 RC and diameter 215mm. The tract radius kept constant at 52mm and disc speed was maintained at 200 rpm resulting in sliding velocity of 1.088 m/s six load, 9.8N, 19.6N, 29.4N, 39.2N, 58.8N, 78.4N wear applied for each materials. The wear tract diameter and disc speed were constant during entire experiment. The wear track diameter and disc speed were kept constant during the entire experiment. Frictional force in kg and cumulative wear loss in mm were measured from the sensor output as a function of time. The wear rates of the pins, defined as the cumulative wear loss suffered by the pin per unit sliding distance per unit load, were calculated from the cumulative wear data. The relative humidity was measured but not controlled and was in the range of 50-55% during the entire test. The worn samples surfaces were cleaned by acetone and examined under the scanning electron microscope.

The specification of the machine is as follows:

Pin diameter: 4, 6, 8, 10, 12 mm.

Disc size: 215 mm diameter and 8 mm thickness.

Disc material: 103 Cri-Eng-31 HRS 60 W62.

Disc rotation: 100-1100 rpm continuously variable with digital tachometer.

Wear track: 180 mm diameter maximum and 50 mm diameter minimum.

Normal load: 1-20 kg.

Friction force: 0-20 kg digital read out with recorder output.

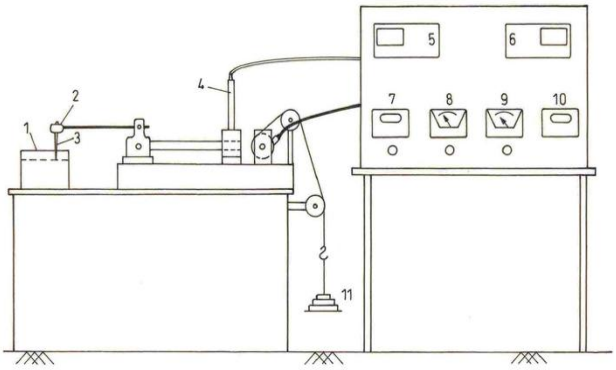

1. Rotating Disc 2. Pin holder 3. Pin

4. Sensor 5. Friction force indicator (kg) 6. Displacement indicator (μm)

7. Speed controller 8. Voltmeter 9. Ammeter

10. Set time meter 11. Load

Fig. 3.6 Schematic diagram of wear testing set up

4.0 Microstructure and Mechanical properties:

4.1 Microstructure and phase identification:

The chapter deals with the effect of different alloying additions on the microstructural features of Mg-Al-Zn-Sn-Pb based alloys processed through conventional casting. Both optical and electron probe micro-analyzer (EPMA)-EDX were used to examine the microstructural feature. The picric acid based etchant (6 g picric acid, 5 ml acetic acid, 100 ml ethanol and 10 ml H_2O) was used to etch the polished specimens. In addition to EDS analysis to identify the phases, XRD analysis was also carried out to confirm the type the phases.

Results and Discussion:

Fig. 4.1 shows XRD patterns of experimental cast alloys H1, H2 and H3. It is found that the main common phases are α –Mg, MgZn, Mg_2Sn, MgAlZn, Mg-Sn-Pb for all alloys. Al_2MM and Mg_2Si, rod-shaped phase are other phases which was found for H2 and H3 respectively based on qualitative analysis of XRD and EPMA-EDX. Mg, Sn and some Pb and Al can be regarded as an intermetallic compound of β-Mg_2Sn, β-Mg_2Al_3, MgZn. The brittle nature of the intermetallic phase and the continuous distribution of the phase weaken the grain boundaries. Cracks are easy to develop and propagate along the grain boundaries, resulting in brittle fractures.

The primary α-Mg phase of this alloy also is dendritic in nature. With 0.5% misch metal addition, the microstructure of Mg-4%Al-3%Zn-3%Sn-3%Pb(H1) alloy does not change much. No peak for β- $Mg_{17}Al_{12}$ is detected. Optical microstructures of the as-

cast alloys H1, H2 and H3 are present in fig. 4.2 respectively. Average grain size is greatly refined by addition of 0.5% MM. (Fig.4.2b). EPMA-EDX micrographs of the alloy are demonstrated in fig 4.3, 4.5 and 4.7 of H1, H2 and H3 respectively. The dark area is Mg matrix. It is observed that precipitates distribute homogeneously along grain boundaries for H1 and H2 alloys. EPMA-EDX analysis is conducted to confirm phases composition. It is found that solid solution of α-Mg that contains mainly mixture of Al, Zn, Sn and Pb. Solubility of La and Ce in Mg is very low at room temperature, thus it is high potential for them to form precipitates during solidification process. From the above result, it is noted there is no Mg-MM or Mg-Al-MM phases is formed. The formation ability from elements to compound can be evaluated by the electro negativity differences between elements. The larger the electro negativity differences are, the easier the formation of a metallic compound is. In addition, diffusion rate of solute atoms is reduced and grain growth is restricted. Due to the crystallography similarity between Mg and Zn, Zn can act as nuclei for Mg during solidification and refine the Mg alloys. The EPMA-EDX micrographs study indicates that the 'Chinese script' Mg_2Si intermetallic contains only Mg and Si. However, variation in composition along its arms is noticed. Higher concentration of Si is noticed at the tip of the arm (Fig. 4.2c).

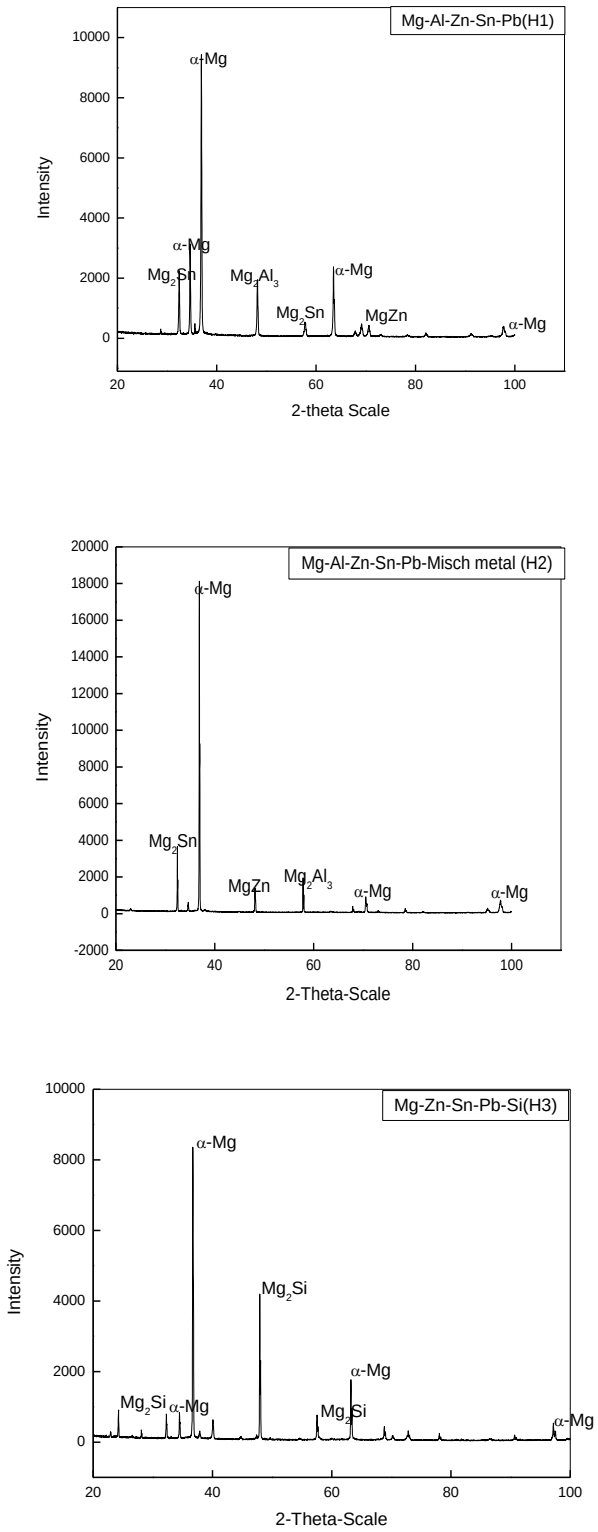

Fig. 4.1 XRD patterns of experimental cast alloys H1, H2 and H3

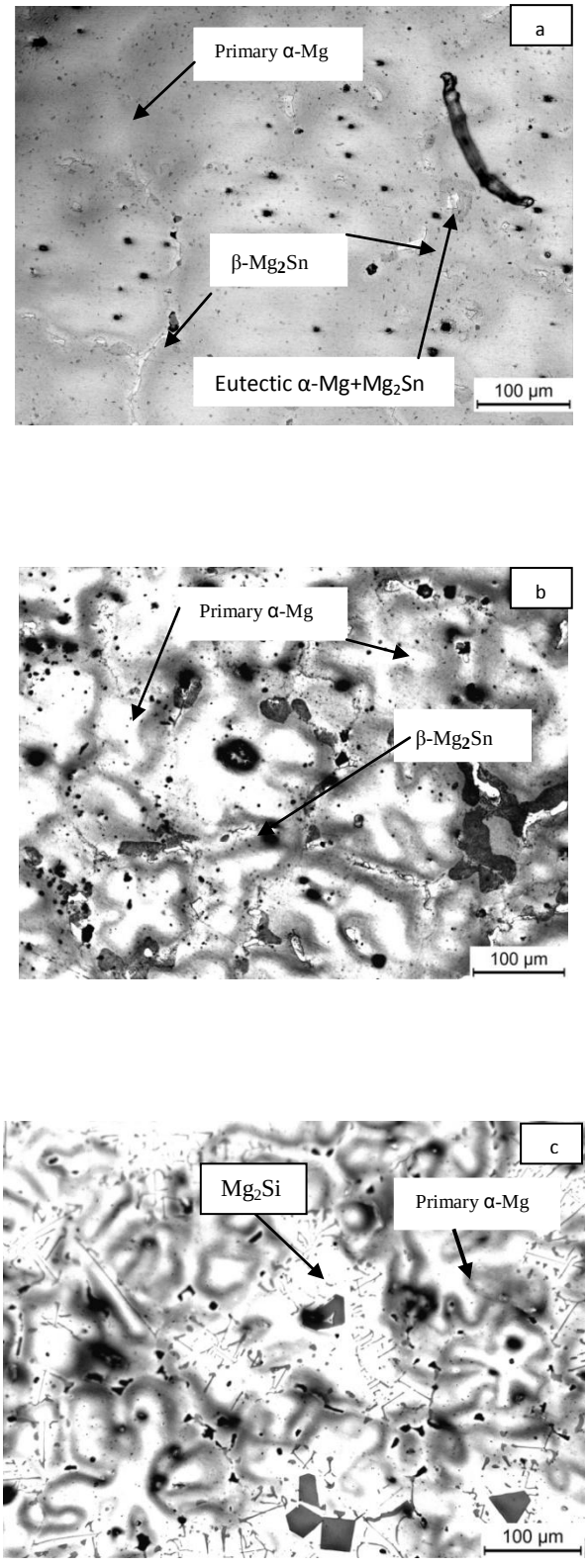

Fig. 4.2 Optical microstructure of a) Mg-4Al-3Zn-3Sn-3Pb (H1) b) Mg-4Al-3Zn-3Sn-3Pb-0.5MM (H2) and c) Mg-3Zn-3Sn-3Pb-2Si (H3) respectively

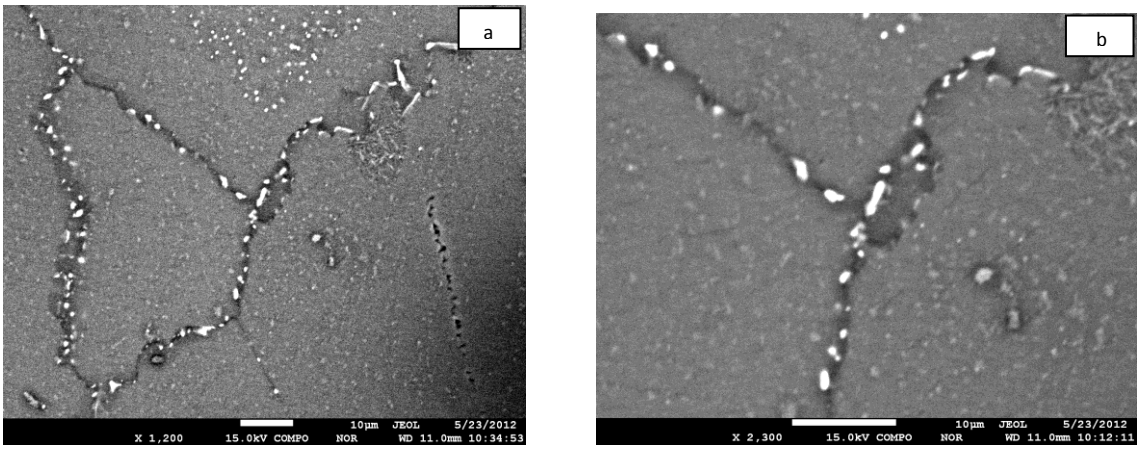

Fig. 4.3 EPMA-EDX micrographs showing different phases in H1alloy; (a) low magnification, and (b) higher magnification

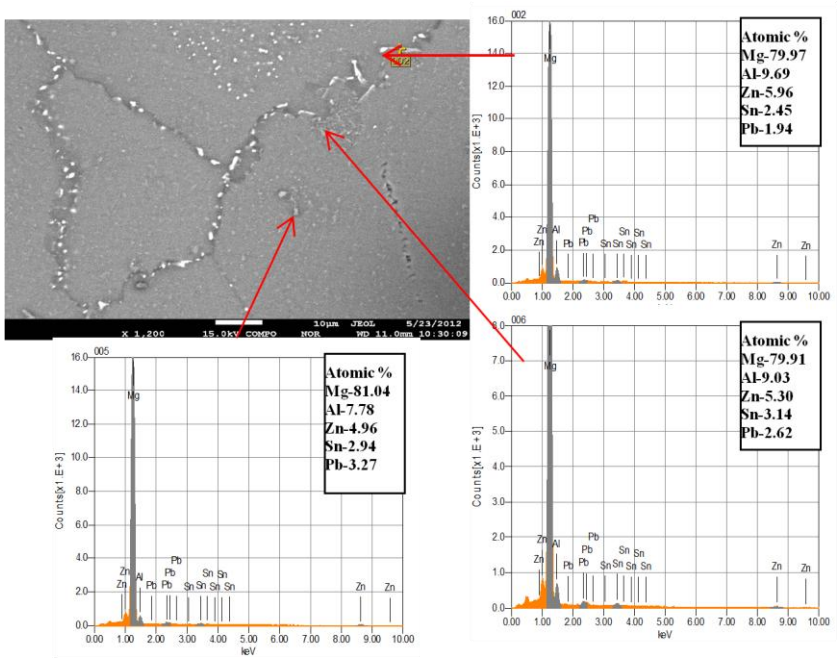

Fig. 4.4 EPMA-EDX micrographs and EDS spectrums of H1 alloy at different regions

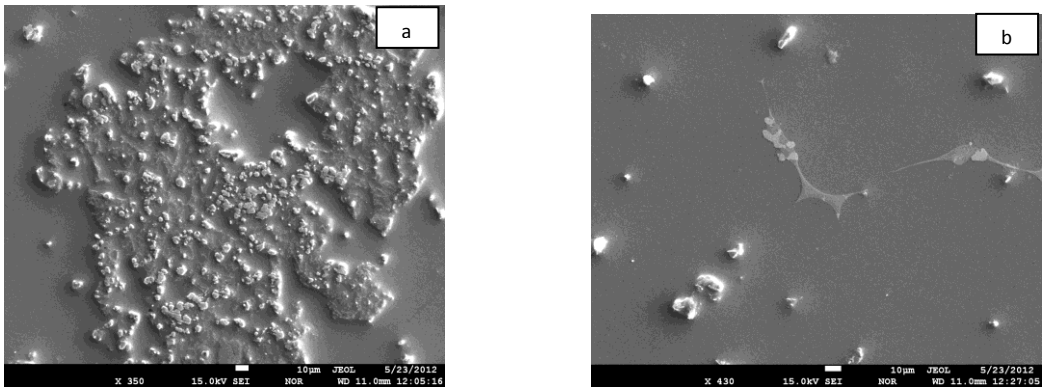

Fig. 4.5 EPMA-EDX micrographs showing different phases in H2 alloy; (a) low magnification, and (b) higher magnification

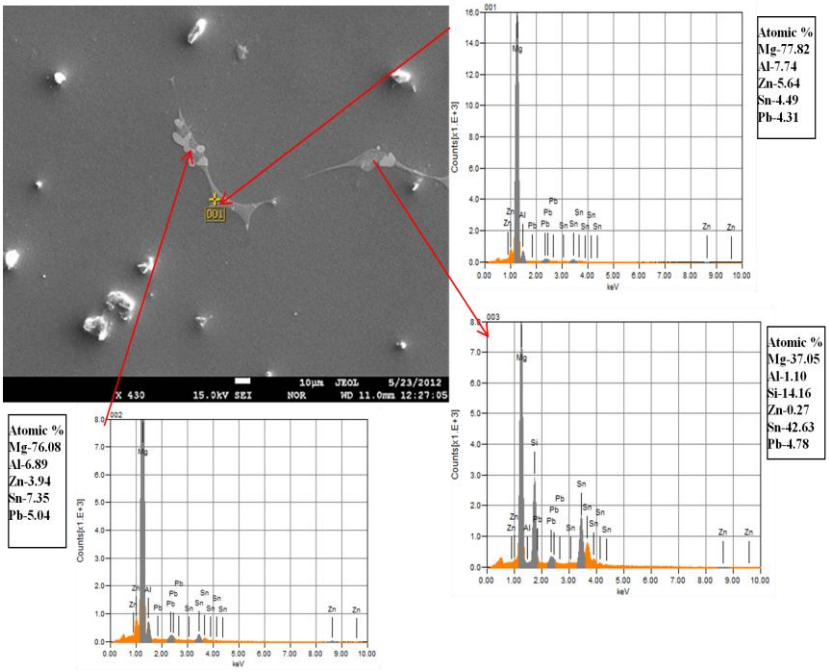

Fig. 4.6 EPMA-EDX micrographs and EDS spectrums of H2 alloy at different regions

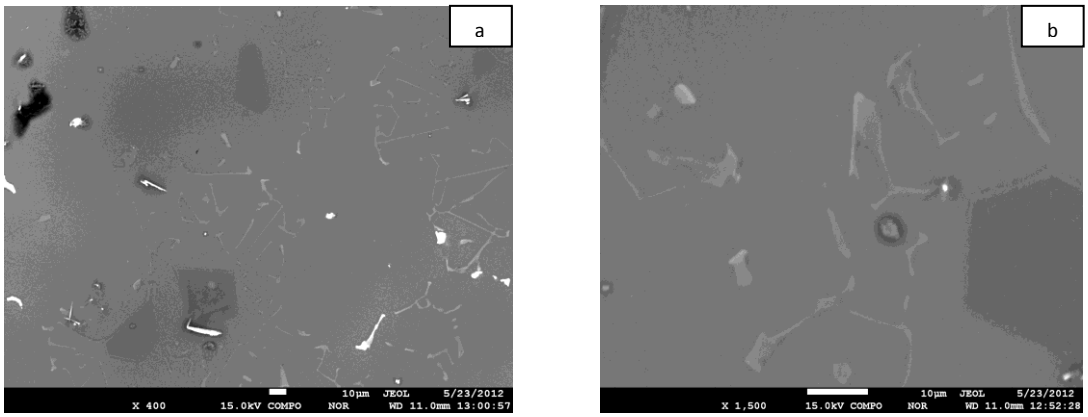

Fig. 4.7 EPMA-EDX micrographs showing different phases in H3 alloy; (a) low magnification, and (b) higher magnification

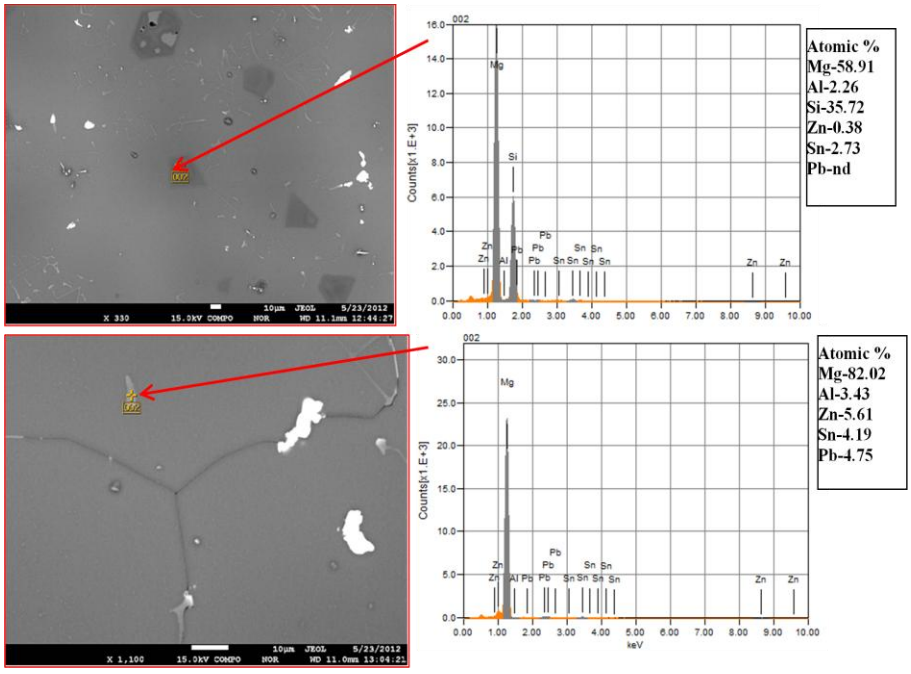

Fig. 4.8 EPMA-EDX micrographs and EDS spectrums of H3 alloy at different regions

Studies on wear properties:

In this chapter, wear properties of Mg-Al-Zn-Sn-Pb based alloy systems have been investigated. As cast samples of conventional alloys were used for wear testing.

Results and Discussion:

Table 5.1 records the alloys investigated for wear behavior by pin-on-disc tests. From the wear tests data on Mg-Al-Zn-Sn-Pb based alloys system, the following aspects of wear were assessed:

(a) Effect of alloying addition the wear characteristics and

(b) Wear mechanism

The density of the alloys was measured by the water displacement technique and hardness reported in Table 5.1. The measured density data of the alloys are close to the theoretical values which indicate that the samples were mostly free from porosity. The microstructures of these alloys are shown in Chapter 4. It can be seen from these photomicrographs that the precipitated phases are uniformly distributed in the Mg matrix. The conventional as cast alloys have a pronounced dendritic matrix structure in which precipitates with different morphologies are distributed. Fig. 5.2 and 5.3 represent the trend of cumulative wear loss in (μm) as a function of sliding distance in meters (m) and under different loads, namely 9.8 N, 19.6 N, 29.4 N and 39.2 N, 58.8 N, 78.4 N for conventional samples, respectively. When the pins are placed on the disc, under pressure the actual contact area is usually very small due to surface roughness. The large localized pressure on the points of real contact (the asperity contacts) can forge

the metallic junctions together even under static conditions due to mechanical alloying effects. Under large load, the real area of contact grows up until it is mostly equal to the nominal area of the pin surfaces resulting in seizure. The average volumetric wear rate (WR) noted from the beginning of the test to any particular stage is expressed as: WR= volumetric wear loss (mm^3)/ [total distance traveled in meters (m) x load applied in Newton (N)]. The values have been calculated for various alloys investigated. The average wear resistance (WRe) is defined as the inverse of the average wear rate and expressed as: WRe = mN/mm^{-3}. The data for average wear rate and wear resistance are indicated in Table 5.2.The average volumetric wear rates fall with the increasing load for all the alloys investigated. The wear resistance, however, increased with the increasing load for all the alloys. In this case no steady state stage was noted during the period of wear test conducted.

Fig 5.1 shows that the cumulative wear loss increases rapidly with the increasing wear load for three alloys. The Mg-Al-Zn-Sn-Pb alloy (H1) offered better wear resistance under all wearing loads investigated as compared to Mg-Al-Zn-Sn-Pb-MM (H2) alloy and to Mg-Zn-Sn-Pb-Si (H3)alloy.(Fig. 5.2 and 5.3(a)). Fig.5.3(a) shows Mg-Al-Zn-Sn-Pb-MM metal alloy shows the highest wear loss at higher loads among all the alloys investigated. The representative graphs of the specific wear rates (defined as volumetric wear loss divided by the corresponding normal force and the sliding distance) as a function of load at room temperature are plotted in Fig. 5.4. The high wear rates in all the alloys at all loads at the initial stage are due to adhesive nature of wear which is associated with high material loss and high value of coefficient of friction (μ). The

cumulative volumetric wear loss and specific wear rates against wear load for all the conventional cast alloys are presented in Figs. 5.3(b) and 5.4 respectively. The cumulative volumetric wear loss increases rapidly with the increasing wear load for the conventional cast as is evident in Figs. 5.3 (b). It is obvious that the volumetric wear loss is more under higher loads due to the increased wearing actions. The variation of frictional co-efficient with sliding distance representative curves for a few alloys system is shown in Fig. 5.5(a). Fig. 5.5(b) shows the average frictional co-efficient at various applied loads for all the conventional cast. It is observed that the co-efficient of friction increases when the load is increased from 9.8 N to 19.6 N for most of the alloys. There are two factors that determine the magnitude of the frictional force, and hence, the co-efficient of friction. These are the mechanical interaction of the surface asperities of the two sliding bodies, and the formation of adhesive junctions at the areas of the contact between the asperities. The increase in co-efficient of friction with increasing load indicates adhesion of the pin to the sliding surface. During the wear run, with increasing load the frictional heat generated is quite appreciable. The localized heating actually facilitates sticking of the pin to the disc surface. The interface temperature increases during dry sliding [48].

In order to investigate the wear mechanism, the surfaces of the worn samples were examined in SEM. The worn out surfaces of the pin materials show diverse topographical features. Most of the worn out surfaces consist of smooth strips, characterized by fine scoring marks. These smooth strips are extended uninterruptedly from one end of the pin specimen to the other. Scoring marks are mostly due to abrasion by the entrapped debris, and work hardened deposits on the counter face [49,50]. The wear loss by scoring mechanism, however, may not lead to a large volume of wear loss since the amount of material removed from a fine groove is quite small .The worn out surfaces of the three alloys (H1,H2,H3) under 9.8 N has shown in (Fig(5.6,5.7,5.8)). It shows the extensive and long continuous grooves on the surfaces parallel to the sliding direction. As the load increases, the width of the corresponding grooves enlarges significantly in comparison (Fig. 5.10) for H3 alloy. Irregular plastic flow lines can be seen indicating the occurrence of extensive plastic deformation during wear run (Fig. 5.7). Cracks and strips of roughened surfaces are also evident on the worn out surface of conventional as cast Mg-3Zn-3Sn-3Pb-2Si (H3) alloy under 58.8 N load (Fig. 5.10(d)). The cracks propagate perpendicular to the sliding directions. Crack nucleation, generally, occurs at some depth below the surface, owing to high hydrostatic compressive pressure acting near the asperity contact [51]. Crack may initiate in the highly work–hardened layer, particularly in the subsurface region. When cracks grow and get interconnected, a layer of material is removed leaving a crater. This is delamination wear. The worn out surfaces of conventional as cast Mg-3Zn-3Sn-3Pb-2Si(H3) alloy at 58.8 N load shows the presence of such evidence (Fig. 5.10(d)).

Under the highest load 78.4 N shows, the mixed mode of wear, i.e. ploughing with local delamination was observed (Fig. 5.10(e)). During wear, the worn out particle debris get agglomerated and stick to the grooved surfaces. The localized heating actually facilitates micro-welding resulting the stick and slip sequence of wear. The interface temperature increases as the wearing couples slides against each other that facilitate sticking of the wear debris at the grooved surfaces [48]. The rise in friction co-efficient with increase in load may be attributed to the enhanced accumulation of wear debris at the pin and disc surface. However, the delaminated wear debris particles formed under higher loads (58.8 N and 78.4 N) are severely work hardened and get fractured so that they do not stick to the sliding surface any further and hence, get removed. Wear debris are generated when a subsurface crack breaks through to the surface. Since the propagating end of the crack (i.e., the crack tip at which the stress is maximum) is always situated behind the moving asperity, the crack reaches the surface after the asperity moves over the crack. SEM micrographs of the worn out surfaces of the pin samples of the conventional cast H1, H2 and H3 alloys tested under 9.8 N loads are presented in (Figs. 5.6-5.8). It is evident from these photomicrographs that the experimental alloys have undergone plastic flow. These alloys also show the presence of distinct grooves, suggesting ploughing on the pin surface. These worn out surfaces are the areas from which the wear debris had been removed. Archard [52] defined adhesive wear volume loss as a function of sliding speed, normal load and materials hardness. This was based on a mechanism of adhesion at the asperities and the

materials removal process related to the cohesive failure of asperities. With the assumption of formation of hemispherical wear particles of the same radius as contact area, Archard [52] developed an equation of wear rate as:

$$W = kLP/3H \quad \text{.....1}$$

where W is volume of materials worn out, k the wear coefficient, L the sliding distance, P the applied load and H is bulk hardness of the materials. The proposed proportionality between the applied load and the wear rate, and the inverse proportionality between hardness and the wear rate were not always observed in sliding wear system.

Table 5.1

Details of the alloys, composition and density values for wear behavior study

Alloy Designation	Alloy composition	Density(g/cc)	Hardness (HV)
H1	Mg-4Al-3Zn-3Sn-3Pb	1.86	53.00
H2	Mg-4Al-3Zn-3Sn-3Pb-0.5MM	1.91	57.00
H3	Mg-3Zn-3Sn-3Pb-2Si	1.908	67.00

MM = Misch Metal

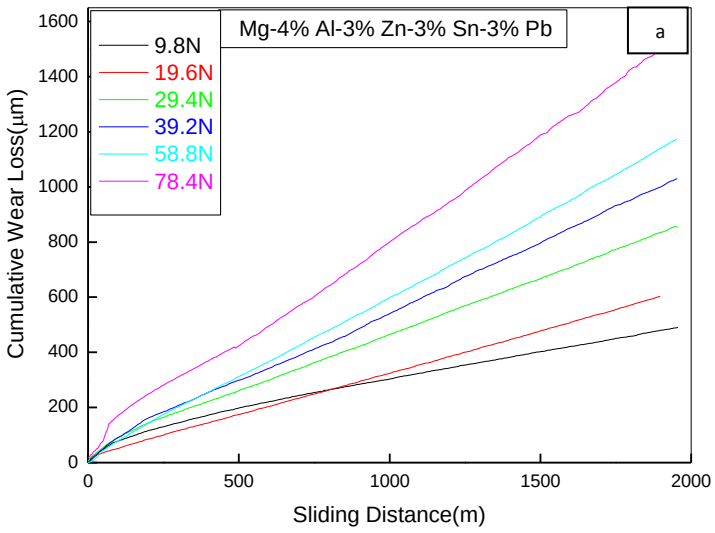

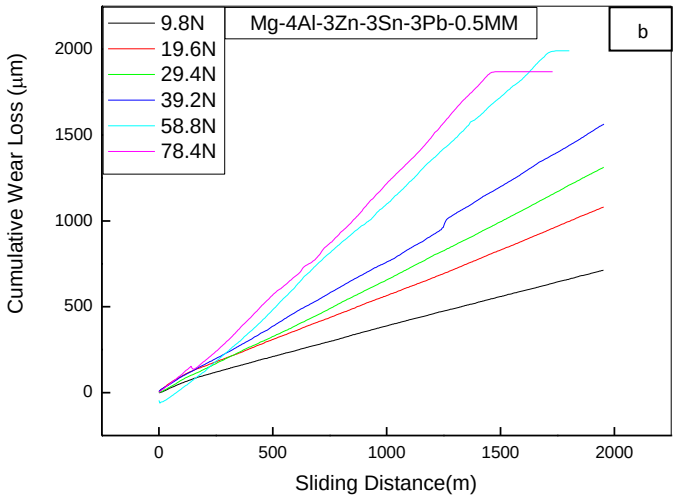

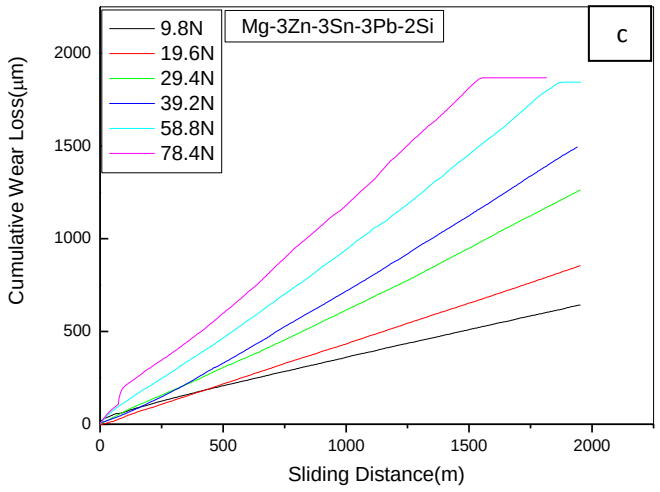

Fig 5.1 Cumulative wear vs sliding distance at different loads of three alloys a) Mg-Al-Zn-Sn-Pb(H1) b) Mg-Al-Zn-Sn-Pb-MM(H2) c) Mg-Zn-Sn-Pb-Si (H3)

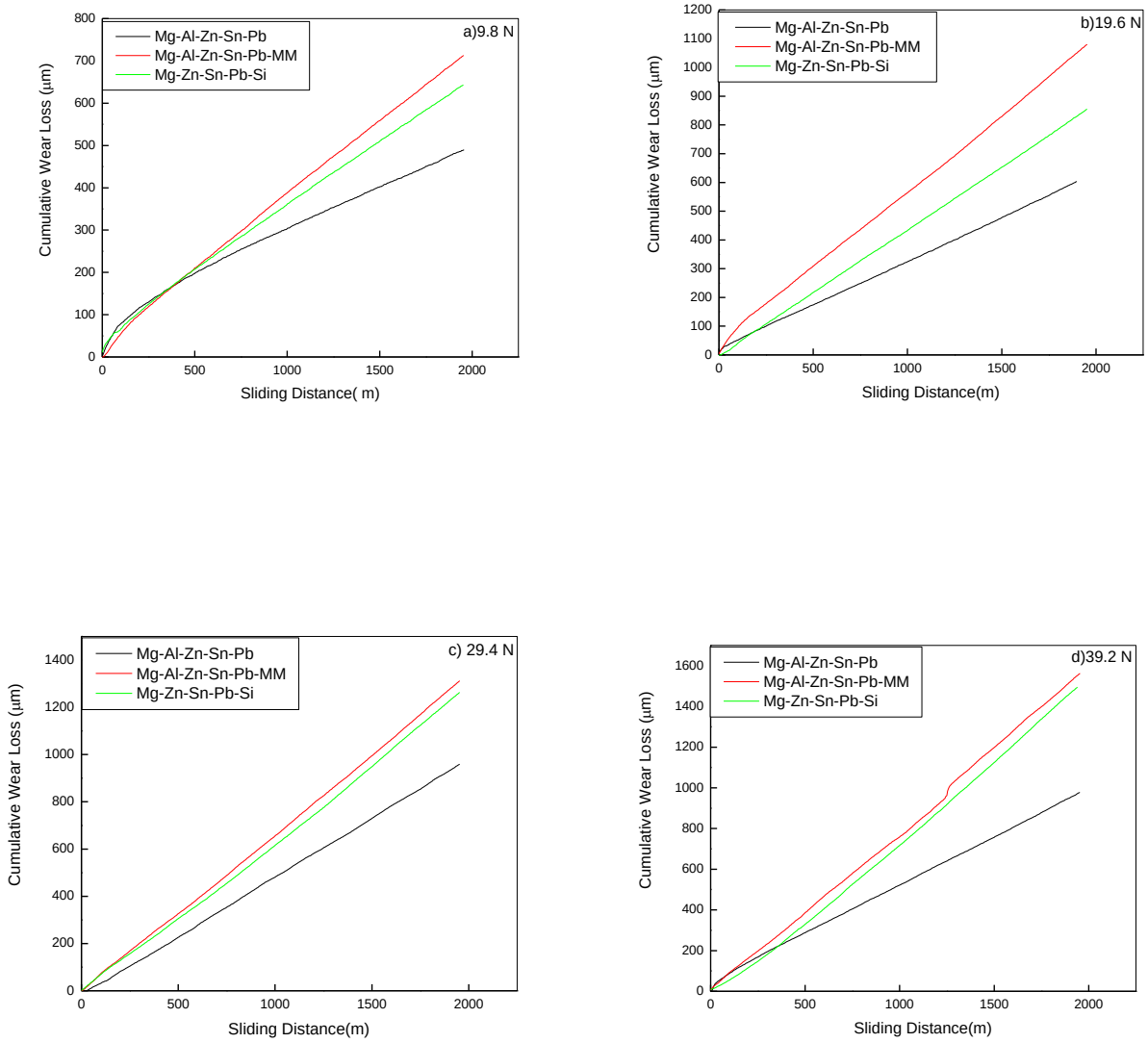

Fig. 5.2 Cumulative wear loss against distance traveled of conventional cast alloys Mg-Al-Zn-Sn-Pb(H1), Mg-Al-Zn-Sn-Pb-MM(H2) and Mg-Zn-Sn-Pb-Si(H3) at different loads; (a) 9.8 N, (b) 19.6 N, (c) 29.4 N, and (d) 39.2 N.

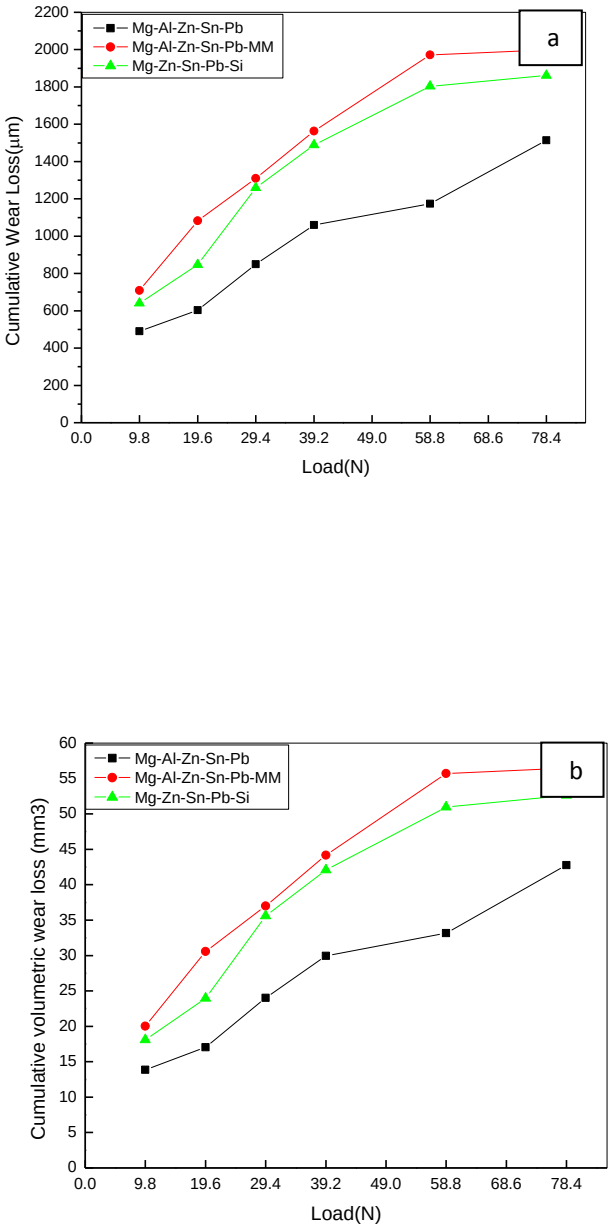

Fig. 5.3 a) Cumulative wear loss and b) Cumulative volumetric wear loss against loads of conventional cast alloys Mg-Al-Zn-Sn-Pb(H1), Mg-Al-Zn-Sn-Pb-MM(H2) , Mg- Zn-Sn- Pb-Si(H3) alloys.

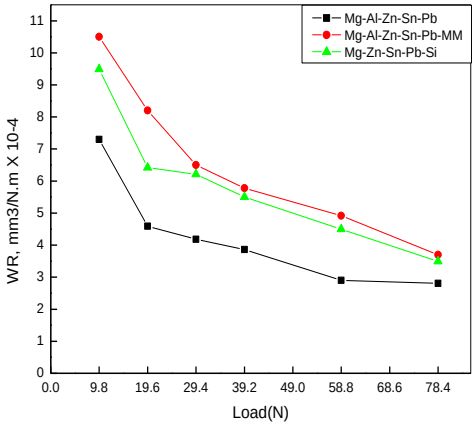

Fig. 5.4 Specific wear rate against loads of conventional cast alloys Mg-Al-Zn- Sn-Pb(H1), Mg-Al-Zn-Sn-Pb-MM(H2) and Mg-Zn-Sn-Pb-Si(H3) alloys.

Table 5.2

Data on wear rate and wear resistance

Alloy Designation	Wear Load											
	9.8N		19.6N		29.4N		39.2N		58.8N		78.4N	
	WR $X10^{-4}$	WRe $X10^{4}$	WR $X10^{-4}$	WRe $X10^{4}$	WR $X10^{-4}$	WRe $X10^{4}$	WR $X10^{-4}$	WRe $X10^{4}$	WR $X10^{-4}$	WRe $X10^{4}$	WR $X10^{-4}$	WRe $X10^{4}$
H1	7.3	0.13	4.59	0.21	4.18	0.23	3.86	0.25	2.9	0.34	2.81	0.35
H2	10.5	0.09	8.2	0.12	6.5	0.15	5.78	0.17	4.92	0.20	3.7	0.27
H3	9.49	0.10	6.42	0.15	6.21	0.16	5.5	0.18	4.5	0.22	3.49	0.28

W.R. = Average volumetric wear rate, $mm^3m^{-1}N^{-1}$

W.Re = Average wear resistance, $N.m/mm^3$

N = Load applied in Newton

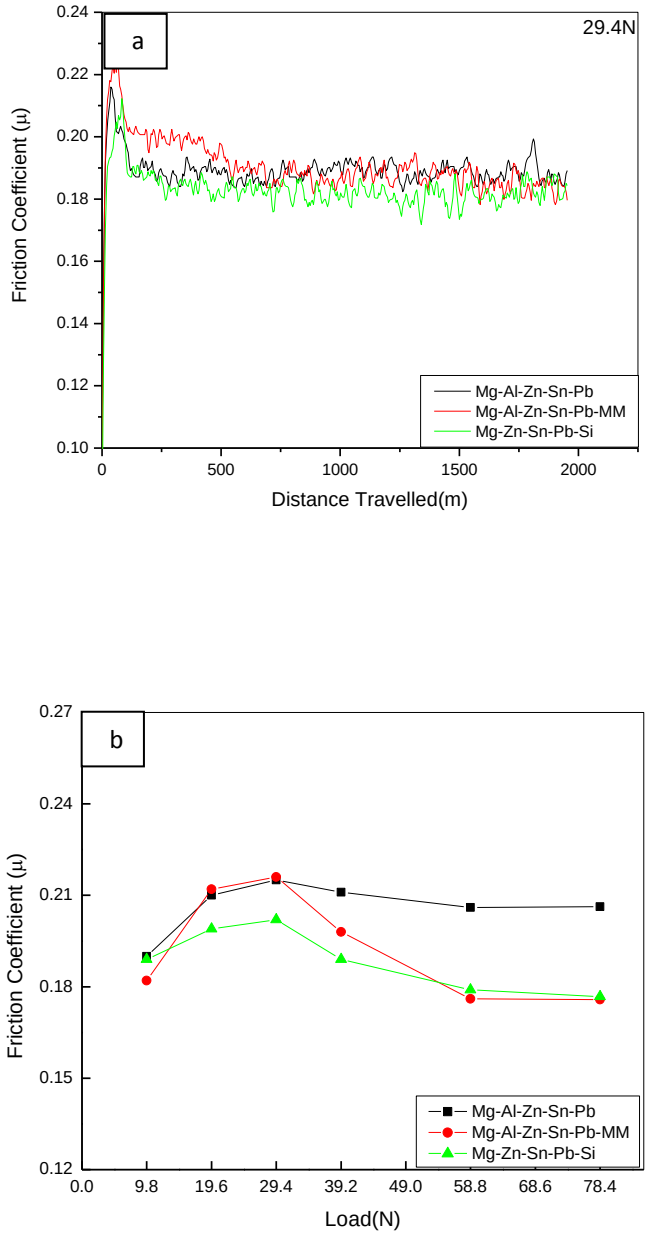

Fig. 5.5 a) Variation of co-efficient of friction against distance traveled at 29.4 N load& b) Variation of friction coefficient against at different loads of conventional cast alloys Mg-Al-Zn-Sn-Pb(H1), Mg-Al-Zn-Sn-Pb-MM(H2) and Mg-Zn-Sn- Pb- Si(H3) alloys.

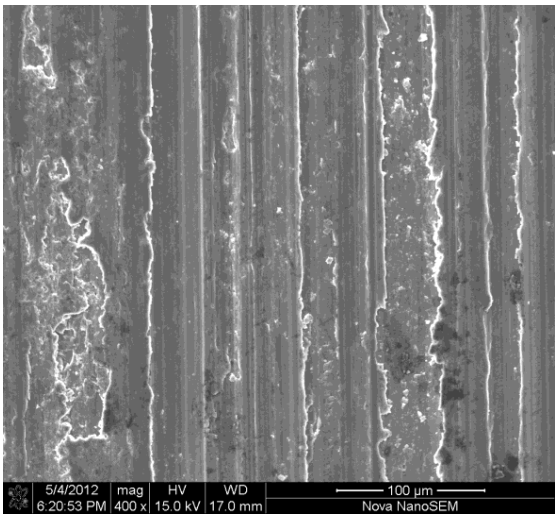

Fig. 5.6 SEM micrographs of worn surfaces of conventional cast Mg-Al-Zn-Sn-Pb (H1) alloy, sliding speed 1.08 ms^{-1}, applied load 9.8 N

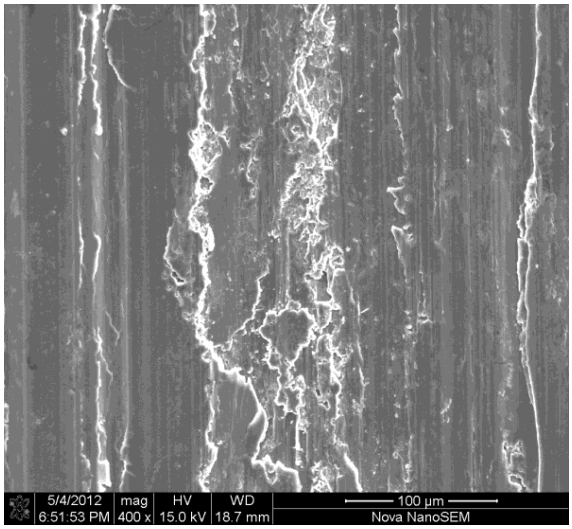

Fig. 5.7 SEM micrographs of worn surfaces of conventional cast Mg-Al-Zn-Sn-Pb-MM (H2) alloy, sliding speed 1.08 ms^{-1},applied load 9.8 N

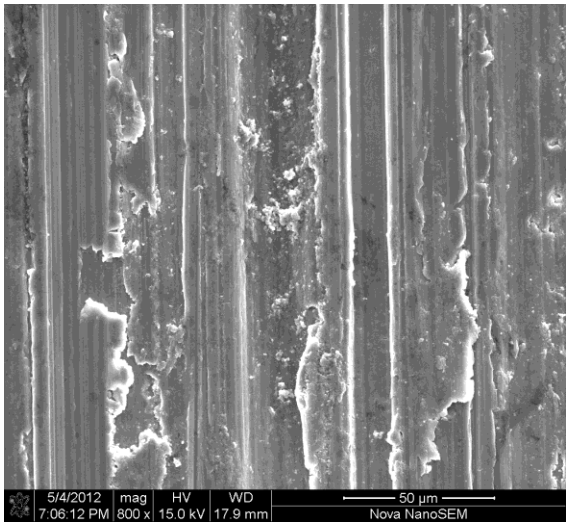

Fig. 5.8 SEM micrographs of worn surfaces of conventional cast Mg-Zn-Sn-Pb-Si(H3) alloy, sliding speed 1.08 ms^{-1}, applied load 9.8 N

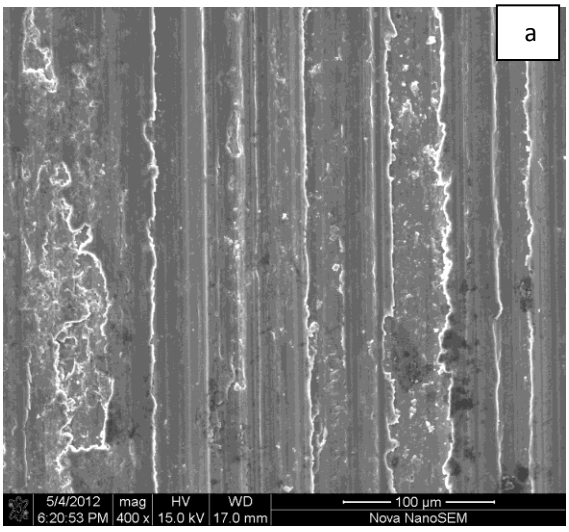

Fig. 5.9 a) SEM micrographs of worn surfaces of conventional cast alloys Mg-Al-Zn-Sn-Pb(H1) at sliding speed 1.08 ms^{-1}, applied load 9.8 N

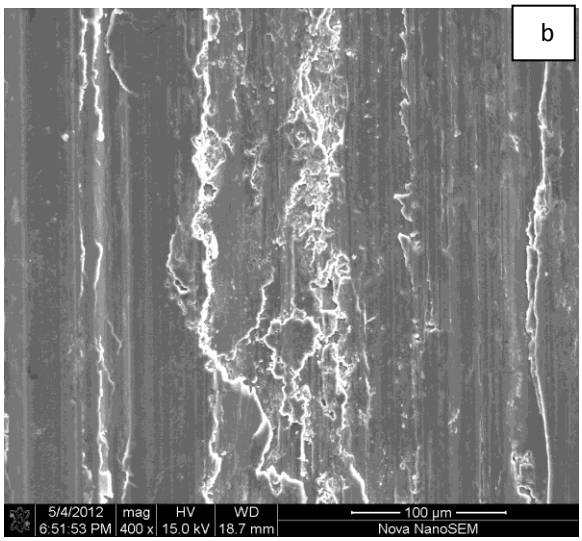

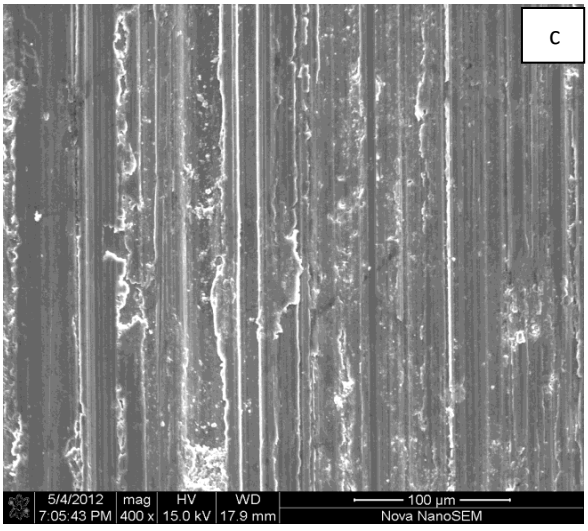

Fig. 5.9 b) SEM micrographs of worn surfaces of conventional cast alloys Mg-Al-Zn-Sn-Pb-MM (H2) and c) Mg-Zn-Sn-Pb-Si(H3) at sliding speed 1.08 ms^{-1},applied load 9.8 N at same magnification

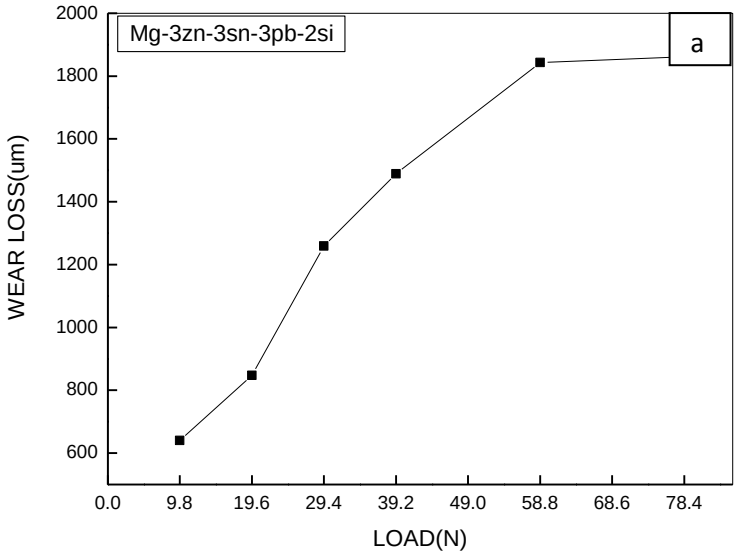

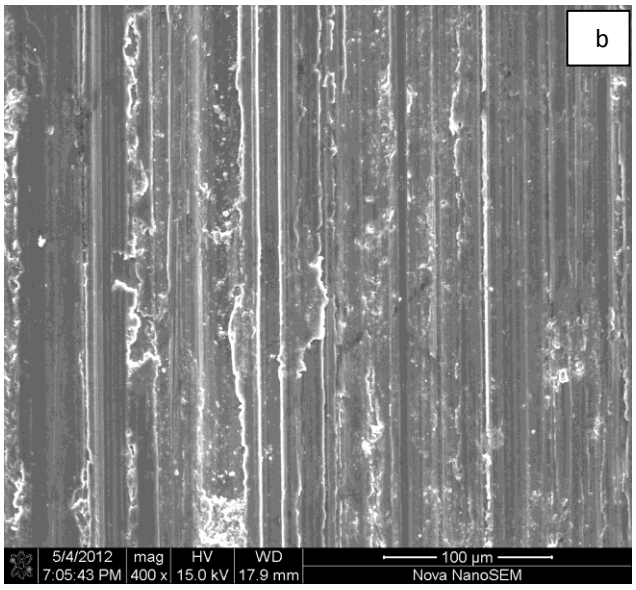

Fig 5.10 a) Wear loss vs load and b) SEM micrographs of worn surfaces of conventional cast alloys Mg-Zn-Sn-Pb-Si (H3) at applied loads 9.8N

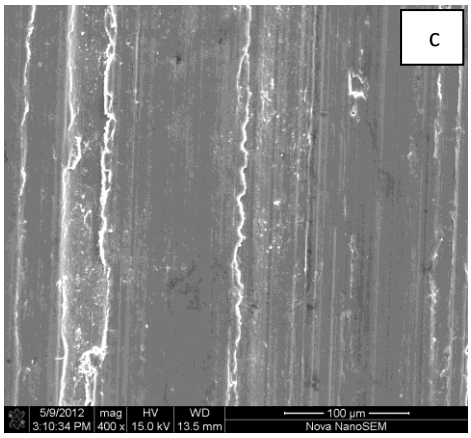

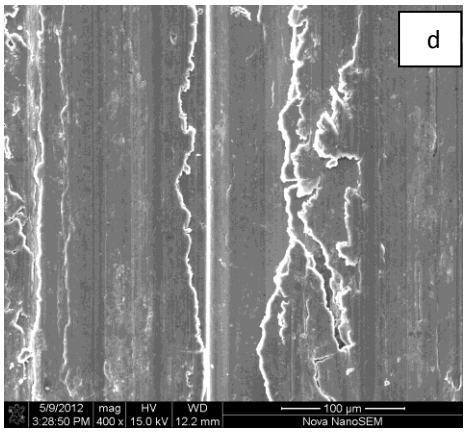

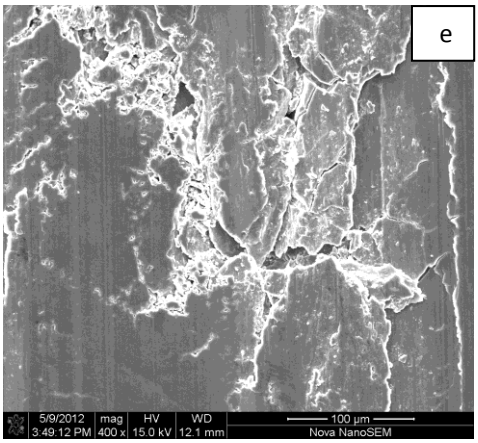

Fig 5.10 SEM micrographs of worn surfaces of conventional cast alloys Mg-Zn-Sn-Pb-Si (H3) at c) 39.2N d) 58.8N e) 78.4N respectively.

4.2 Mechanical properties:

In this chapter, mechanical properties of Mg-Al-Zn-Pb-Sn alloys based system with alloying addition are reported.

4.2.1 Solution treatment:

All the alloys were subjected to solution treatment was carried out in order to homogenize the alloys. A sand bed prepared using carbon charcoal and dry silica sand with a volume ratio of 25:75 was placed in the muffle furnace. Samples were placed in a mild steel tray in such way that no piece touches others. The charcoal-silica sand mixture was also put in the tray burying the samples. This helped to evacuate oxygen present in the furnace during heat treatment. This procedure was found satisfactory to avoid the oxidation of magnesium samples during the heat treatment. The samples were solution heat treatment at 410^0C for 8-10 h depending upon sample thickness followed by immediate water quenching at room temperature.

4.2.2 Tensile properties:

Variation in microstructure influences the tensile properties of Mg-based alloys to a significant extent. Therefore, the tensile properties of Mg-Al-Zn-Pb-Sn based alloys with different alloying were investigated and presented in this section. Tensile samples were prepared according to ASTM E8 standard. The tests were carried out as-cast and heat treated conditions at room temperature for all the alloys and

processing conditions. The average value of three tensile test data was reported in this work. In order to evaluate the % elongation during room temperature testing extensometer was used.

Figure 4.9, presents the ultimate tensile strength (UTS), yield strength (YS) and percentage of elongation(%E) of Mg-4%Al-3%Zn-3%Sn-3%Pb(H1), Mg-4%Al-3%Zn-3%Sn-3%Pb-0.5%MM (H2) and Mg-3%Zn-3%Sn-3%Pb-3% Si (H3) alloys measured from the tensile test carried out at room temperatures. The mechanical properties of three alloys were listed in Table 4.1. As it is clear from data, alloy H2 exhibits the best strength but more the % elongation for alloy H1. The addition of MM greatly improves the mechanical properties of the studied alloys. This is due to the formation of intermetallics which contains rare earth elements. The UTS and elongation of H2 alloy are about 40%, and 100 % higher than those of H3 alloy. Firstly, it is noted from Fig 4.2 that with addition of MM, the grain structure is greatly refined. According to the Hall-petch relation, the mechanical properties of the studied alloys can be enhanced through grain- refining strengthening effect. During tensile test, dislocations movement and grain boundaries sliding can be effectively prohibited. Clearly without addition of aluminum and MM alloy H3 shows very poor strength and % elongation.

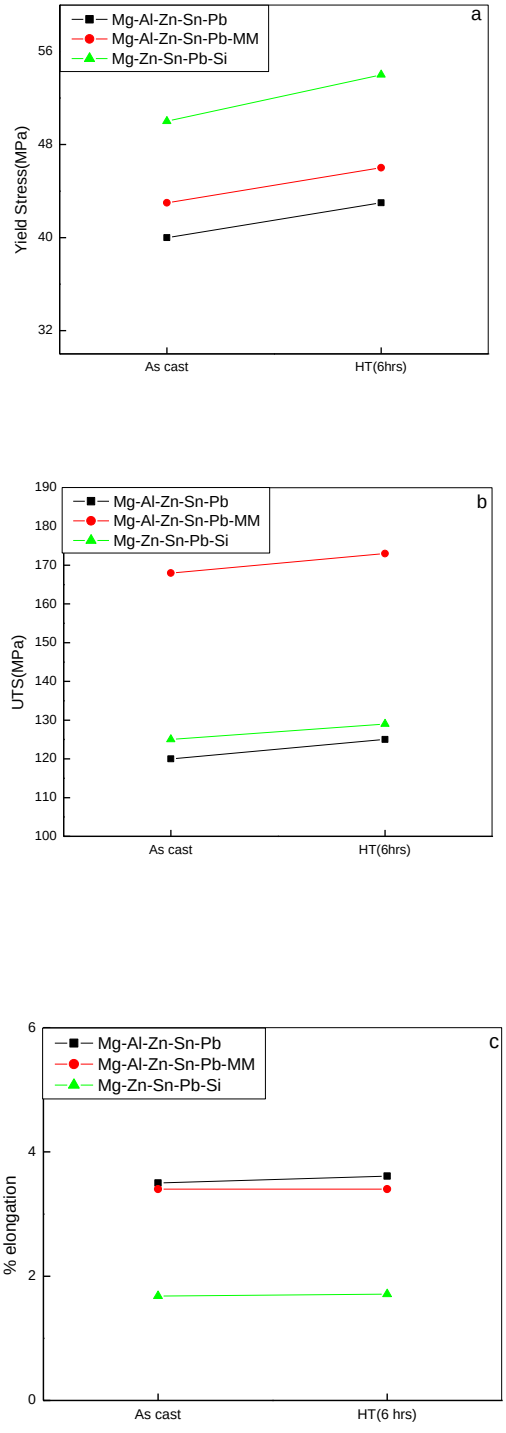

Fig 4.9 Tensile properties of alloys at room temp a) Yield strength b) UTS c) Percentage elongation)

Table 4.1

Tensile properties data of alloys at room temp

Alloy	Yield strength (MPa)	Tensile strength(MPa)	% elongation
HI	42	122	3.6
H2	44	170	3.4
H3	52	127	1.69

4.2.3 Fractography studies of tensile specimen

To understand the fracture mechanism, broken tensile specimens have been examined under scanning electron microscopy (SEM). Fig. 4.10, 4.11 and 4.12 shows fractured surface of H1, H2 and H3 alloys at room temperature respectively. The fracture surface consists of secondary crack, cleavage plane river pattern and dimples .Small cleavage steps can also be found in some areas. Consequently, the tensile fracture surface has mixed characteristics of cleavage and quasi-cleavage fracture. A minute tearing ridge and tough dimples can be observed. Since Mg is having HCP crystal structure and thus, the failure of Mg is expected to be brittle fracture in the mode of cleavage or quasi-cleavage. Microcracks are developed in cleavage fracture, along certain crystal planes, which is normally (0001) in case with Mg. A large number of cleavage planes are seen in the fracture surface with cleavage steps of different sizes and river patterns in Fig. 4.10 and 4.11 for H1 and H2 alloys respectively, but more dimples has been found for H3 alloy (Fig. 4.12).

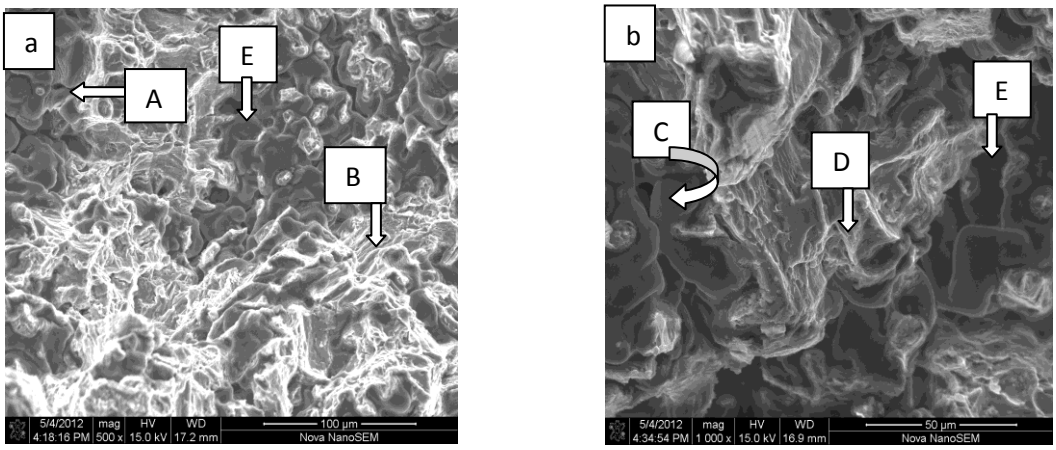

Fig 4.10 SEM Tensile fractorgraph of Mg-4%Al-3%Zn-3%Sn-3%Pb (H1) alloy at room temp. (A) Secondary crack (B) river pattern (C) cleavage plane (D) plastic deformation (E) dimples at (a) Lower magnification (b) Higher magnification

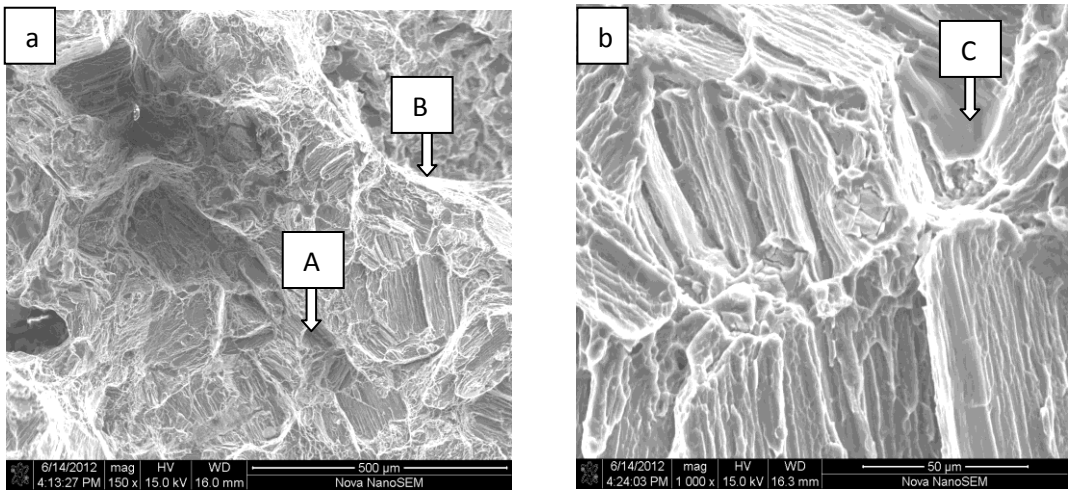

Fig 4.11 Tensile fractograph of Mg-Al-Zn-Sn-Pb-MM alloy (H2) at room temperature for at (a) Lower magnification (b) Higher magnification

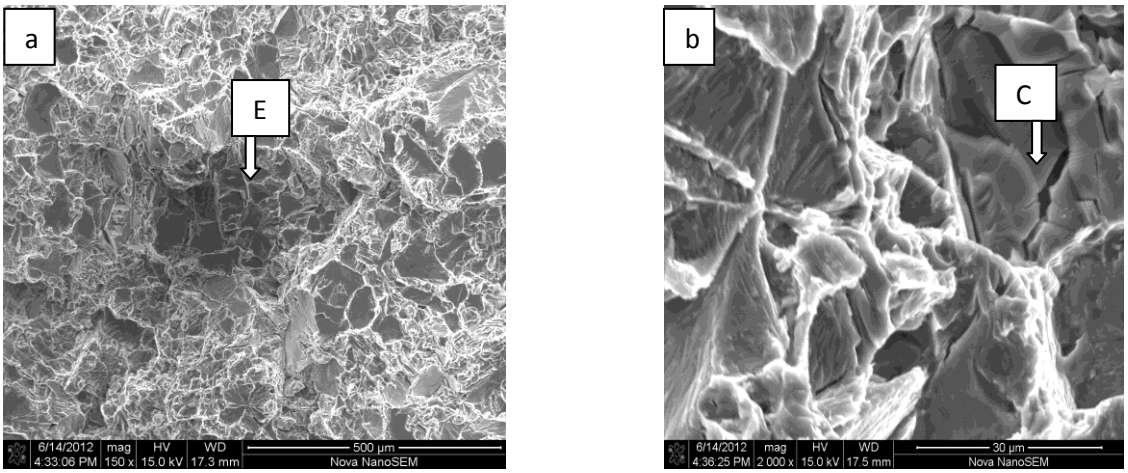

Fig 4.12 Tensile fractograph of of Mg-Zn-Sn-Pb-Si alloy (H3) at room temperature for at (a) Lower magnification (b) Higher magnification

4.3 Hardness:

Fig. 4.14 shows the hardness of studied alloys as-cast and in heat treated condition. It has been found that hardness value of Mg-3Zn-3Sn-3Pb-2Si (H3) is more than that of H1 and H2 as-cast condition as well as in heat treated condition.

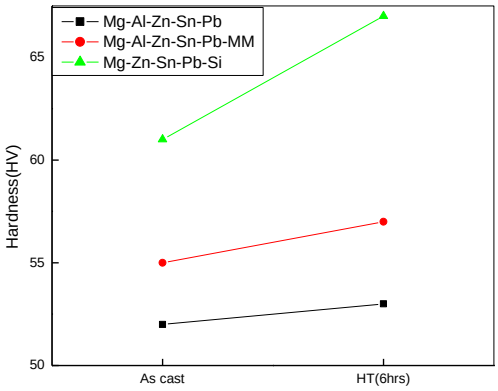

Fig 4.13 Hardness of Mg-based alloys system as cast and heat treated condition

Table 4.2

Details of the alloys, composition, and hardness value as cast and in heat treated condition

Alloy Designation	Alloy composition	Hardness (HV)	
		As cast	Heat treated
H1	Mg-4Al-3Zn-3Sn-3Pb	52	53
H2	Mg-4Al-3Zn-3Sn-3Pb-0.5MM	55	57
H3	Mg-3Zn-3Sn-3Pb-2Si	61	67

MM= Misch Metal (Purity;52%Ce-26%La-16%Nd-6%Pr)

6.0 Conclusions

In the present research work the additions of MM and Si to conventional cast Mg-Al-Zn-Sn-Pb based alloys have been carried out. Their effects on the microstructure, tensile properties, hardness and wear behaviour are studied. This chapter summarizes all the major observations and the conclusions drawn from this study as well as highlights the significant contributions of this thesis to the existing knowledge.

1. The microstructure of the studies alloys Mg-4Al-3Zn-3Sn-3Pb (H1) and Mg-4Al-3Zn-3Sn-3Pb-0.5MM (H2) are dendritic in nature while for Mg-3Zn-3Sn-3Pb-2Si (H3) the 'Chinese script' Mg_2Si intermetallic structure is obtained.
2. Effect of misch metal on microstructure and mechanical properties as-cast Mg-4Al- 3Zn-3Sn-3Pb-0.5MM (H2) is maximum. The result shows that Misch metal addition leads to obvious grain refinement.
3. The alloys investigated exhibit plastic deformation and work hardening during wear test.
4. The co-efficient of friction increases when load increases from 9.8 to 29.4N.
5. Specific wear rate (mm^3/N-m) or cumulative wear loss (mm^3) is found maximum for Mg-4Al-3Zn-3Sn-3Pb-0.5MM (H2) vice versa wear resistance is minimum for H2.
6. Mg-4Al-3Zn-3Sn-3Pb-0.5MM (H2) alloy exhibit the best mechanical properties.

7. The UTS and elongation of Mg-4Al-3Zn-3Sn-3Pb-0.5MM (H2) alloy are about 40% and 100 % higher than that of H3 alloy.
8. The UTS, YS, and percentage elongation of H2 alloy are 170MPa, 44MPa and 3.4%.
9. The 'Chinese script' Mg_2Si intermetallic is found in Mg-3Zn-3Sn-3Pb-3Si (H3) alloy.
10. The vicker hardness value is found maximum for Mg-3Zn-3Sn-3Pb-2Si (H3) is 67 HV.

6.1 AVENUES FOR FUTURE WORK:

The growth of magnesium alloys is driven primarily by the automotive industry as structural material due to increasing environmental concerns and severe government regulations on CO_2 emissions. Therefore, the need of light weight metallic materials which will have sufficient strength and ductility has led to significant consideration of materials researchers into Mg-alloys because of their low density and high specific strength. But, the greatest limitation for the usage of Mg alloy is its poor formability at room temperature.

Therefore, across the globe researchers are putting their effort to prepare highly ductile Mg-based alloys for suitable application in structural areas including automobiles. By varying the alloying elements one can control the structures including the grain refinement for obtaining optimized properties. The mechanical working (rolling and forging) of Mg alloys is a challenging task and has a good scope for further research.

1. A. A. Luo, and M. O. Pekguleryuz, 1994, "Cast Magnesium alloys for elevated temperature" J. Mater. Sci, 29, 5259-5271.
2. C. S. Roberts, 1960 "Magnesium and its alloys" John Wiley and Sons Inc., 85-87.
3. M. Regev, E. Aghion, A. Rosen, and M. Bamberger, 1998 "Creep studies of coarse grained AZ91D Magnesium alloy" Mater. Sci. Eng. A, 252, 6-16.
4. http://www.ford.com/servlet/ecmcs/ford/index
5. P.D. Caton: 1992 "Proc. magnesium alloys and their applications" 367
6. D. Eliezer, E. Aghion, and F. H. Froes, 1997 "The Science, Technology, and Applications of Magnesium" 343-354.
7. ASM metal hand book, 1990 ,10th edition, 2, 457
8. Y. Wang, B. Sun, Q. Wang, Y. Zhu, and W. Ding, 2002 " An understanding of the hot tearing mechanism in AZ91 magnesium alloy" Mater. Letters, 53, 35-39.
9. D. Wenwen, S. Yangshan, M. Xuegang, X. Feng, Z. Min, and D. Wu, 2003 "Microstructure and mechanical properties of Mg–Al based alloy with calcium and rare earth additions" Mater. Sci. Eng., 356, 1-7.
10. P. Bakke, and H. Westengen, 2003 "Die casting for high performance—Focus on alloy development" Adv. Eng. Mat., 5, 879-885.
11. A. K. Dahle, D. H. St John, and G. L. Dunlop, 2000 "Development and challenges in the utilization of magnesium alloys" Mater. Forum, 24, 167-182.
12. I. J. Polmear, 1992 "Proc. magnesium alloys and their application" Eds. B. L.Mordike, and F. Hehmann, Garmisch-Partenkirchen, Germany, 201-212.
13. M. O. Pekguleyuz, 2000 ,Mater. Sci. Forum, 350-351, 131-140.
14. T. B. Massalski, 1986 "Binary alloy phase diagram" 1, 1567.

15. Z. P. Luo, D. Y. Song, and S.Q. Zhang, 1995 "Strengthening effects of rare-earths on wrought Mg-Zn-Zr-RE alloys" J. Alloys and Compounds, 230, 109-114.
16. M. Suzuki, H. Sato, K. Maruyama, and H. Oikawa, 1998 "Creep behavior and deformation microstructure of Mg-Y alloys at 550K" Mater. Sci. Eng. A, 252, 248
17. K. Maruyama, M. Suzuki, and H. Sato, 2002 "Creep strength of magnesium-based alloys" Metall. Mater. Trans. A, 33, 875-882.
18. P. Abachi, A. Masoudi, and K. Purazrang, 2006, Mater. Sci. Eng. A, 435, 653-657.
19. Pekguleryuz, M O, Kaya A A, 2003 "Creep resistant Magnesium alloys for power train applications" Advance Engineering Materials, 5(12), 866
20. E.F.Emley, 1966 "Principle of Magnesium Technology" Pergamon press, First edition, 925
21. M. O. Pekguleryuz, M. M. Avedesiaan, and Sainte-Foy, 1992 "Proc. Magnesium alloys and their applications" Eds., B. L. Mordike, F. Hehmann, , Germany, 213-220
22. A. K. Dahle, Young C. Lee, mark D. Nave, Paul L. Schaffer and David H. St John, 2001 "Development of the as-cast microstructure in magnesium-aluminium alloys" J Light Metal, 1, 61-72, 439, 653-657
23. A.A.Nayeb-Hashemi and J.B.clark, Bull, 1984 "Alloy phase Diagrams" 5(5)
24. A.A.Nayeb-Hashemi and J.B.clark, Bull, 1984 "Alloy phase Diagrams" 5(4)
25. A.A.Nayeb-Hashemi and J.B.clark, Bull, 1984 "Alloy phase Diagrams" 5(6)
26. A.A.Nayeb-Hashemi and J.B.clark, Bull, 1984 "Alloy phase Diagrams" 6(1)
27. Wang Jianli, Shi Ning, Cao Zhanyi, 2010 " Effect of zinc and misch metal on microstructure and mech. properties of Mg-Al-Mn alloy" J rare earths, 28(5), 794

28. E. F. Emley, 1966 “Principle of magnesium technology” Pergamon press, 1st edition, 218-240.
29. ASM Hand book, Casting, 1998 ASM International, 4th edition, 15, 798-803.
30. S. C. Erickson, 1998 “Foundry Manag.Technol” 126, 38-49.
31. M. O. Pekguleyuz: 2000, Mater. Sci. Forum, 350-351, 131-140.
32. H. Friedrich and S. Schumann, 2001 “Research for a “new age of magnesium” in the automotive industry” J Mater Proc Tech, 117,276-281.
33. S. Celotto, 2000 “TEM study of continuous precipitation in Mg–9 wt%Al–1 wt%Zn alloy” Acta Mater., 48, 1775-1787.
34. E. Aghion, N. Moscovitch and A. Arnon, 2007 “The correlation between wall thickness and properties of HPDC Magnesium alloys” Mater. Sci. Eng. A, 447,341-346.
35. C. D. Lee, 2007 “ Effect of grain size on the tensile properties of magnesium alloy” Mater. Sci. Eng. A, 459, 355-360.
36. M. K. Surappa, E. Blank and J. C. Januet, 1986 “Effect of Macro-Porosity on the Strength and Ductility of Cast Al-7Si-0.3Mg alloy” Scripta Metall., 20, 1281-1286
37. S.Jayalakshmi, S. V. Kailas and S. Seshan, 2003 , J Mater. Sci., 38, 1383-89
38. Koichi Ishikawa, Hiroyuki Watanabe and Toshiji Mukai, 2005 “High strain rate deformation behavior of an AZ91 magnesium alloy at elevated temperatures” Mater. Lett. 59, 1511- 1515.
39. K. Kubota, M. Mabuchi and K. Higashi, 1999, J Mater. Sci., 34, 2255-2262.

40. T. Mohri, M. Mabuchi, and M. Nakamura, 1999 “Microstructure and mechanical properties of a Mg-4Y-3RE alloy processed by thermo-mechanical treatment” Mater. Sci. Eng., A257, 287.

41. Y. H. Wei, Q. D. Wang, Y. P. Zhu, W. J. Ding, Y. Chino and M. Mabuchi, 2003 “Super plasticity and grain boundary sliding in rolled AZ91 magnesium alloy at high strain rates” Mater. Sci. Eng., 360, 107-115

42. K. Hiratsuka, A. Enomoto, and T. Sasada, 1992 “Friction and wear of Al_2O_3, ZrO_2 and SiO_2 rubbed against pure metals” Wear, 153, 361-373.

43. A. Alahelisten, F. Bergman, M. Olsson and S. Hogmark, 1993 “On the wear of aluminium and magnesium metal matrix composites” Wear, 165, 221-226

44. H. Chen, and A.T. Alpas, 2000 “Sliding wear map for the magnesium alloy Mg–9Al–0.9Zn (AZ91)” Wear, 246, 106-116.

45. Magnesium Electron Limited, 1992” Magnesium alloy database, MATUS Databases, Engineering Information Co. Ltd,.

46. A.K. Dahle, D. H. St John and G. L. Dunlop, 2000 “ Developments and challenges in the utilisation of Magnesium alloys” Materials Forum, 24,167-182.

47. D. Eliezer, E. Aghion, and F.H. Froes, 1998 “Advanced Performance Materials, 5, 201-212.

48. R. T. Spurr, 1979 “Temperatures reached during sliding” 55, 289-293.

49. B. N. Pramila Bai, S. K. Biswas, 1991 “Effect of load on dry sliding wear of aluminium-silicon alloys” Acta Metall. Mater., 39, 833-840.

50. A. S. Reddy, B. N. Pramila Bai, K. S. S Murthy,and S. K. Biswas, 1995 “Mechanism of seizure of aluminium-silicon alloys dry sliding against steel” Wear, 181-183, 658-667.

51. S. Jahanmir, and N. P. Suh, 1997 “Mechanics of subsurface void nucleation in delamination” wear, 44, 17-38

52. J.F.Archard, 1953 “Mechanics of subsurface void nucleation in delamination wear” J.Appl.Phys., 24, 981-988